

1 **Evaluating Data Assimilation Algorithms**

2 K. J. H. LAW * AND A. M. STUART

Warwick Mathematics Institute, University of Warwick, Coventry, UK

arXiv:1107.4118v4 [physics.data-an] 25 Mar 2012

* *Corresponding author address:* Kody J. H. Law, Warwick Mathematics Institute, University of Warwick, Coventry CV4 7AL, UK.

E-mail: k.j.h.law@warwick.ac.uk

ABSTRACT

3
4 Data assimilation leads naturally to a Bayesian formulation in which the posterior probability
5 distribution of the system state, given all the observations on a time window of interest,
6 plays a central conceptual role. The aim of this paper is to use this Bayesian posterior
7 probability distribution as a gold standard against which to evaluate various commonly used
8 data assimilation algorithms.

9 A key aspect of geophysical data assimilation is the high dimensionality and limited
10 predictability of the computational model. We study the 2D Navier-Stokes equations in a
11 periodic geometry, which has these features and yet is tractable for explicit and accurate com-
12 putation of the posterior distribution by state-of-the-art statistical sampling techniques. The
13 commonly used algorithms that we evaluate, as quantified by the relative error in reproduc-
14 ing moments of the posterior, are 4DVAR and a variety of sequential filtering approximations
15 based on 3DVAR and on extended and ensemble Kalman filters.

16 The primary conclusions are that *under the assumption of a well-defined posterior prob-*
17 *ability distribution:* (i) with appropriate parameter choices, approximate filters can perform
18 well in reproducing the mean of the desired probability distribution; (ii) however they do
19 not perform as well in reproducing the covariance; (iii) the error is compounded by the need
20 to modify the covariance, in order to induce stability. Thus, filters can be a useful tool in
21 predicting mean behavior, but should be viewed with caution as predictors of uncertainty.
22 These conclusions are intrinsic to the algorithms when assumptions underlying them are not
23 valid and will not change if the model complexity is increased.

24 1. Introduction

25 The positive impact of data assimilation schemes on numerical weather prediction (NWP)
26 is unquestionable. Improvements in forecast skill over decades reflect not only the increased
27 resolution of the computational model, but also the increasing volumes of data available,
28 and the increasing sophistication of algorithms to incorporate this data. However, because
29 of the huge scale of the computational model, many of the algorithms used for data assimila-
30 tion employ approximations, based on both physical insight and computational expediency,
31 whose effect can be hard to evaluate. The aim of this paper is to describe a method of
32 evaluating some important aspects of data assimilation algorithms, by comparing them with
33 a gold-standard: the Bayesian posterior probability distribution on the system state given
34 observations. In so doing we will demonstrate that carefully chosen filters can perform
35 well in predicting mean behaviour, but that they typically perform poorly when predicting
36 uncertainty, such as covariance information.

37 In typical operational conditions the observed data, model initial conditions, and model
38 equations are all subject to uncertainty. Thus we take the perspective that the gold standard,
39 which we wish to reproduce as accurately as possible, is the (Bayesian) posterior probability
40 distribution of the system state (possibly including parameters) given the observations. For
41 practical weather forecasting scenarios this is not computable. The two primary competing
42 methodologies for data assimilation that *are* computable, and hence are implemented in
43 practice, are *filters* Kalnay (2003) and *variational methods* Bennett (2002). We will compare
44 the (accurately computed, extremely expensive) Bayesian posterior distribution with the
45 output of the (approximate, relatively cheap) filters and variational methods used in practice.
46 Our underlying dynamical model is the 2D Navier-Stokes equations in a periodic setting.
47 This provides a high dimensional dynamical system, which exhibits a range of complex
48 behaviours, yet which is sufficiently small that the Bayesian posterior may be accurately
49 computed by state-of-the-art statistical sampling in an off-line setting.

50 The idea behind filtering is to update the posterior distribution of the system state

51 sequentially at each observation time. This may be performed exactly for linear systems
52 subject to Gaussian noise, and is then known as the Kalman filter Kalman (1960); Harvey
53 (1991). For nonlinear or non-Gaussian scenarios the particle filter Doucet et al. (2001) may
54 be used and provably approximates the desired probability distribution as the number of
55 particles is increased Bain and Crişan (2008). However in practice this method performs
56 poorly in high dimensional systems Snyder et al. (2008) and, whilst there is considerable
57 research activity aimed at overcoming this degeneratation van Leeuwen (2010); Chorin et al.
58 (2010); Bengtsson et al. (2003), it cannot currently be viewed as a practical tool within the
59 context of geophysical data assimilation. In order to circumvent problems associated with
60 the representation of high dimensional probability distributions some form of Gaussian ap-
61 proximation is typically used to create practical filters. The oldest and simplest such option
62 is to use a nonlinear generalization of the mean update in the Kalman filter, employing a
63 constant prior covariance operator, obtained offline through knowledge coming from the un-
64 derlying model and past observations Lorenc (1986); this methodology is sometimes refered
65 to as *3DVAR*. More sophisticated approximate Gaussian filters arise from either lineariz-
66 ing the dynamical model, yielding the *extended Kalman filter* Jazwinski (1970), or utilizing
67 ensemble statistics, leading to the *ensemble Kalman filter* Evensen et al. (1994); Evensen
68 (2003). Information about the underlying local (in time) Lyapunov vectors, or bred vec-
69 tors (see Kalnay (2003) for discussion) can be used to guide further approximations that
70 are made when implementing these methods in high dimensions. We will also be interested
71 in the use of *Fourier diagonal filters*, introduced in Harlim and Majda (2008); Majda et al.
72 (2010), which approximate the dynamical model by a statistically equivalent linear dynam-
73 ical system in a manner which enables the covariance operator to be mapped forward in
74 closed form; in steady state the version we employ here reduces to a particular choice of
75 3DVAR, based on climatological statistics. An overview of particle filtering for geophysical
76 systems may be found in Van Leeuwen (2009) and a quick introduction to sequential filtering
77 may be found in Arulampalam et al. (2002).

78 Whilst filtering updates the system state sequentially each time when a new observation
79 becomes available variational methods attempt to incorporate data which is distributed over
80 an entire time-interval. This may be viewed as an optimization problem where the objective
81 function is to choose the initial state, and possibly forcing to the physical model, in order
82 to best match the data over the specified time-window. As such it may be viewed as a
83 PDE-constrained optimization problem Hinze et al. (2008), and more generally as a partic-
84 ular class of regularized inverse problem Vogel (2002); Tarantola (2005); Banks and Kunisch
85 (1989). This approach is referred to as 4DVAR in the geophysical literature, when the
86 optimization is performed over just the initial state of the system Talagrand and Courtier
87 (1987); Courtier and Talagrand (1987) and as weak constraint 4DVAR when optimization is
88 also over forcing to the system Zupanski (1997).

89 From a Bayesian perspective, the solution to an inverse problem is statistical, rather than
90 deterministic, and is hence significantly more challenging: regularization is imposed through
91 viewing the unknown as a random variable, and the aim is to find the posterior probability
92 distribution on the state of the system on a given time window, given the observations on
93 that time window. With the current and growing capacity of computers it is becoming
94 relevant and tractable to begin to explore such approaches to inverse problems in differential
95 equations Kaipio and Somersalo (2005), even though it is currently infeasible to do so for
96 NWP. There has, however, been some limited study of the Bayesian approach to inverse
97 problems in fluid mechanics using path integral formulations in continuous time as introduced
98 in Apte et al. (2007); see Apte et al. (2008a,b); Quinn and Abarbanel (2010); Cotter et al.
99 (2011) for further developments. We will build on the algorithmic experience contained in
100 these papers here. For a recent overview of Bayesian methodology for inverse problems in
101 differential equations, see Stuart (2010), and for the Bayesian formulation of a variety of
102 inverse problems arising in fluid mechanics see Cotter et al. (2009). The key take home
103 message of this body of work on Bayesian inverse problems is that it is often possible to
104 compute the posterior distribution of state given noisy data with high degree of accuracy,

105 albeit at great expense: the methodology could not be used online as a practical algorithm,
106 but provides us with a gold-standard against which we can evaluate on-line approximate
107 methods used in practice.

108 There are several useful connections to make between the Bayesian posterior distribu-
109 tion, filtering methods and variational methods all of which serve to highlight the fact that
110 they are all *attempting* to represent related quantities. The first observation is that, in the
111 linear Gaussian setting, if backward filtering is implemented on a given time window (this is
112 known as *smoothing*) after forward filtering, then the resulting mean is equivalent to 4DVAR
113 Fisher et al. (2005). The second observation is that the Bayesian posterior distribution at
114 the end of the time window, which is a non-Gaussian version of the Kalman smoothing
115 distribution just described, is equal to the exact filtering distribution at that time, provided
116 the filter is initialized with the same distribution as that chosen at the start of the time
117 window for the Bayesian posterior model Stuart (2010). The third observation is that the
118 4DVAR variational method corresponds to maximizing the Bayesian posterior distribution
119 and is known in this context as a MAP estimator Cox (1964); Kaipio and Somersalo (2005).
120 More generally, connections between filtering and smoothing have been understood for some
121 time Bryson and Frazier (1963).

122 For the filtering and variational algorithms implemented in practice, these connections
123 may be lost, or weakened, because of the approximations made to create tractable algorithms.
124 Hence we attempt to evaluate these algorithms by their ability to reproduce moments of the
125 Bayesian posterior distribution since this provides an unequivocal notion of a perfect solution,
126 given a complete model description, including sources of error; we hence refer to it as the gold
127 standard. We emphasize that we do not claim to present optimal implementations of any
128 method except the gold standard MCMC. Nonetheless, the phenomena we observe and the
129 conclusions we arrive at will not change qualitatively if the algorithms are optimized. They
130 reflect inherent properties of the approximations used to create online algorithms useable in
131 practical online scenarios.

132 The ability of filters to track the signal in chaotic systems has been the object of study in
133 data assimilation communities for some time and we point to the paper Miller et al. (1994)
134 as an early example of this work, confined to low dimensional systems, and to the more
135 recent Carrassi et al. (2008) for study of both low and high dimensional problems, and for
136 further discussion of the relevant literature. As mentioned above, we develop our evaluation
137 in the context of the 2D Navier Stokes equations in a periodic box. We work in parameter
138 regimes in which at most $O(10^3)$ Fourier modes are active. This model has several attractive
139 features. For instance, it has a unique global attractor with a tunable parameter, the viscosity
140 (or, equivalently the Reynolds number), which tunes between a one-dimensional stable fixed
141 point and very high-dimensional strongly chaotic attractor Temam (2001). As the dimension
142 of the attractor increases, many scales are present, as one would expect in a model of the
143 atmosphere. By working with dimensions of size $O(10^3)$ we have a model of significantly
144 higher dimension than the typical toy models that one encounters in the literature Lorenz
145 (1996, 1963). Therefore, while the 2D Navier-Stokes equations do not model atmospheric
146 dynamics, we expect the model to exhibit similar predictability issues as arise atmospheric
147 models, and this fact, together their high dimensionality, makes them a useful model with
148 which to study aspects of atmospheric data assimilation. However we do recognize the need
149 for follow-up studies which investigate similar issues for models such as Lorenz-96, or quasi-
150 geostrophic models, which can mimic or model the baroclinic instabilities which drive so
151 much of atmospheric dynamics.

152 The primary conclusions of our study are that: (i) with appropriate parameter choices,
153 approximate filters can perform well in reproducing the mean of the desired probability
154 distribution; (ii) however these filters typically perform poorly when attempting to reproduce
155 information about covariance as the assumptions underlying them may not be valid (iii) this
156 poor performance is compounded by the need to modify the filters, and their covariance in
157 particular, in order to induce filter stability and avoid divergence. Thus, whilst filters can be
158 a useful tool in predicting mean behaviour, they should be viewed with caution as predictors

159 of uncertainty. These conclusions are intrinsic to the algorithms and will not change if the
160 model is more complex, for example resulting from a smaller viscosity in our model. We
161 reiterate that these conclusions are based on our assumption of well-defined initial prior,
162 observational error, and hence Bayesian posterior distributions. Due to the computational
163 cost of computing the latter we look only at one, initial, interval of observations, but upon
164 our assumption, the accuracy over this first interval will limit accuracy on all subsequent
165 intervals, and they will not become better. Under the reasonable assumption that the process
166 has finite correlation time, the initial prior will be forgotten eventually and, in the present
167 context, this effect would be explored by choosing different priors coming from approximation
168 of the asymptotic distribution by some filtering algorithm and/or climatological statistics
169 and testing the robustness of conclusions, and indeed of the filtering distribution itself, to
170 changes in prior. The question of sensitivity of the results to choice of prior is not addressed
171 here. We also restrict our attention here to the perfect model scenario.

172 Many comparisons of various versions of these methods have been carried out recently.
173 For example, Meng and Zhang (2010); Zhang et al. (2010) compare EnKF forecast with
174 3DVAR and 4DVAR(without updated covariance) in the Weather Research and Forecast-
175 ing (WRF) model. In their real-data experiments, they conclude that EnKF and 4DVAR
176 perform better with respect the Root Mean Square Error (RMSE), while the EnKF forecast
177 performs better for longer lead times. This result is consistent with ours, although it could be
178 explained by an improved approximation of the posterior distribution at each update time.
179 Our results indicate 4DVAR could perform better here, as long as the approximate filtering
180 distribution of 4DVAR with the propagated Hessian is used. Of course this is too expensive
181 in practice and often a constant covariance is used; this will limit performance in reproduc-
182 ing the statistical variation of the posterior filtering distribution for prior in the next cycle.
183 This issue is addressed partially in Meng and Zhang (2010); Zhang and Zhang (2012), where
184 EnKF is coupled to 4DVAR and the covariance comes from the former, while the mean is
185 updated by the latter, and the resulting algorithm outperforms either of the individual ones

186 in the RMSE sense. Two fundamental classes of EnKFs were compared theoretically in the
187 large ensemble limit in Lei et al. (2010), and it was found that the stochastic version (the
188 one we employ here) in which observations are perturbed is more robust to perturbations
189 in the forecast distribution than the deterministic one. Another interesting comparison was
190 undertaken in Hamill et al. (2000) in which several ensemble filters alternative to EnKF in
191 operational use are compared with respect to RMSE as well as other diagnostics such as
192 rank histograms Anderson (1996). We note that over long times the RMSE values for the
193 algorithms we consider are in the same vicinity as the errors between the estimators and the
194 truth that we present at the single filtering time.

195 The rest of the paper will be organized in the following sections. First, we introduce
196 the model and inverse problem in section 2, then we describe the various methods used to
197 (approximately) compute posterior smoothing and filtering distributions in section 3. Then
198 we describe the results of the numerical simulations in two sections. The first, section 4,
199 explores the accuracy of the filters by comparison with the posterior distribution and the
200 truth. The second, section 5, explains the manifestation of instability in the filters, describes
201 how they are stabilized, and studies implications for accuracy. We provide a summary
202 and conclusions in section 6. In the Appendix 7 we describe some details of the numerical
203 methods.

204 **2. Statement of the Model**

205 In this section we describe the dynamical model, and the filtering and smoothing prob-
206 lems which arise from assimilating data into that model. The discussion is framed prior to
207 discretization. Details relating to numerical implementation may be found in the Appendix
208 7.

210 The dynamical model we will consider is the two-dimensional incompressible Navier-
 211 Stokes equation in a periodic box with side of length two. By projecting into the space
 212 of divergence-free velocity fields, this may be written as a dynamical equation for the
 213 divergence-free velocity field u with the form

$$214 \quad \frac{du}{dt} + \nu Au + F(u) = f, \quad u(0) = u_0. \quad (1)$$

215 Here A (known as the Stokes operator) models the dissipation and acts as a (negative)
 216 Laplacian on divergence free fields, $F(u)$ the nonlinearity arising from the convective time-
 217 derivative and f the body force, all projected into divergence free functions. We also work
 218 with spatial mean-zero velocity fields as, in periodic geometries, the mean evolves indepen-
 219 dently of the other Fourier modes. See Temam (2001) for details concerning the formulation
 220 of incompressible fluid mechanics in this notation. We let \mathcal{H} denote the space of square-
 221 integrable, periodic and mean-zero divergence-free functions on the box. In order that our
 222 results are self-contained apart from the particular choice of model considered, we define the
 223 map $\Psi(\cdot; t) : \mathcal{H} \rightarrow \mathcal{H}$ so that the solution of (1) satisfies

$$224 \quad u(t) = \Psi(u_0; t). \quad (2)$$

225 Equation (1) has a global attractor and the viscosity parameter ν tunes between regimes
 226 in which the attractor is a single stationary point, through periodic, quasi-periodic, chaotic,
 227 and strongly chaotic (the last two being delicate to distinguish between). These regimes are
 228 characterized by an increasing number of positive Lyapunov exponents, and hence increas-
 229 ing dimension of the unstable manifold. In turn, this results in a system which becomes
 230 progressively less predictable. This tunability through all predictability regimes, coupled to
 231 the possibility of high dimensional effective dynamics which can arise for certain parameter
 232 regimes of the PDE, makes this a useful model with which to examine some of the issues
 233 inherent in atmospheric data assimilation.

234 *b. Inverse Problem*

235 The basic inverse problem which underlies data assimilation is to estimate the state of
 236 the system, given the model dynamics for the state, together with noisy observations of
 237 the state. In our setting, since the model dynamics are deterministic, this amounts to
 238 estimating the initial condition from noisy observations at later times. This is an ill-posed
 239 problem which we regularize by adopting a Bayesian approach to the problem, imposing
 240 a prior Gaussian random field assumption on the initial condition. Throughout it will be
 241 useful to define $\|\cdot\|_B = \|B^{-\frac{1}{2}} \cdot\|$ for any covariance operator B and we use this notation
 242 throughout the paper, in particular in the observation space, with $B = \Gamma$ and in the initial
 243 condition space with $B = \mathcal{C}_0$.

244 Our prior regularization on the initial state is to assume

$$245 \quad u_0 \sim \mu_0 = \mathcal{N}(m_0, \mathcal{C}_0). \quad (3)$$

246 The prior mean m_0 is our best guess of the initial state, before data is acquired (background
 247 mean) and the prior covariance \mathcal{C}_0 (background covariance) regularizes this by allowing
 248 variability with specified magnitude at different length-scales. The prior covariance $\mathcal{C}_0 : \mathcal{H} \rightarrow$
 249 \mathcal{H} is self-adjoint and positive, and is assumed to have summable eigenvalues, a condition
 250 which is necessary and sufficient for draws from this prior to be square integrable.

251 Now we describe the noisy observations. We observe only the velocity field, and not the
 252 pressure. Let $\Gamma : \mathcal{H} \rightarrow \mathcal{H}$ be self-adjoint, positive operators and let

$$253 \quad y_k \sim \mathcal{N}(u(t_k), \Gamma) \quad (4)$$

254 denote noisy observations of the state at time $t_k = kh$ which, for simplicity of exposition
 255 only, we have assumed to be equally spaced. We assume independence of the observational
 256 noise: $y_k|u_k$ is independent of $y_j|u_j$ for all $j \neq k$; and the observational noise is assumed
 257 independent of the initial condition u_0 .

258 For simplicity and following convention in the field, we will not distinguish notationally
 259 between the random variable and its realization, except in the case of the truth, which will

260 be important to distinguish by u^\dagger in subsequent sections in which it will be simulated and
 261 known. The inverse problem consists of estimating the posterior probability distribution of
 262 $u(t)$, given noisy observations $\{y_k\}_{k=0}^j$, with $j \leq J$. This is referred to as

- 263 • *Smoothing* when $t < t_j$;
- 264 • *Filtering* when $t = t_j$;
- 265 • *Predicting* when $t > t_j$.

266 Under the assumption that the dynamical model is deterministic, the smoothing distribution
 267 at time $t = 0$ can be mapped forward in time to give the exact filtering distribution, which in
 268 turn can be mapped forward in time to give the exact predicting distribution (and likewise
 269 the filtering distribution mapped backward, if the forward map admits an inverse, yields
 270 the smoothing distribution). If the forward map were linear, for instance in the case of the
 271 Stokes equation ($F(u) = 0$), then the posterior distribution would be Gaussian as well, and
 272 could be given in closed form via its mean and covariance. In the nonlinear case, however,
 273 the posterior cannot be summarized through a finite set of quantities such as mean and
 274 covariance and, in theory, requires infinitely many samples to represent. In the language of
 275 the previous section, as the dimension of the attractor increases with Reynolds number, the
 276 nonlinearity begins to dominate the equation, the dynamics become less predictable, and the
 277 inverse problem becomes more difficult. In particular, Gaussian approximations can become
 278 increasingly misleading. We will see that sufficient nonlinearity for these misleading effects
 279 can arise more than one way, via the dynamical model or the observational frequency.

280 1) SMOOTHING

281 We start by describing the Bayesian posterior distribution, and link this to variational
 282 methods. Let $u_k = u(kh)$, $\Psi(u) = \Psi(u; h)$, and $\Psi^k(\cdot) = \Psi(\cdot; kh)$. Furthermore, define the

283 conditional measures for $j_1, j_2 \leq J$

$$284 \quad \mu_{j_1 j_2}(u_{j_1}) = \mathbb{P}(u_{j_1} | \{y_k\}_{k=0}^{j_2}).$$

285 (For notational convenience we do not distinguish between a probability distribution and its
 286 density, using μ and \mathbb{P} interchangeably for both). The posterior distributions are completely
 287 characterized by the dynamical model in Eq. (2) and by the random inputs given in Eq. (4)
 288 and Eq. (3).

We focus on the posterior distribution $\mu_{0|J}$ since this probability distribution, once known, determines $\mu_{j|J}$ for all $J \geq j \geq 0$ simply by using (2) to map the probability distribution at time $t = 0$ into that arising at any later time $t > 0$. Bayes' rule gives a characterization of $\mu_{0|J}$ via the ratio of its density with respect to that of the prior ¹:

$$\frac{\mathbb{P}(u_0 | \{y_k\}_{k=0}^J)}{\mathbb{P}(u_0)} = \frac{\mathbb{P}(\{y_k\}_{k=0}^J | u_0)}{\mathbb{P}(\{y_k\}_{k=0}^J)}$$

289 so that

$$290 \quad \frac{\mu_{0|J}(u)}{\mu_0(u)} \propto \exp\{-\Phi(u)\},$$

291 where

$$292 \quad \Phi(u) = \frac{1}{2} \left(\sum_{k=0}^J \|y_k - \Psi^k(u)\|_{\Gamma}^2 \right).$$

293 The constant of proportionality is independent of u and irrelevant for the algorithms that
 294 we use below to probe the probability distribution $\mu_{0|J}$. Note that here, and in what follows,
 295 u denotes the random variable u_0 .

296 Using the fact that the prior μ_0 is Gaussian it follows that the *maximum a posteriori*
 297 (*MAP*) estimator of $\mu_{0|J}$ is the minimizer of the functional

$$298 \quad I(u) = \Phi(u) + \frac{1}{2} \|u - m_0\|_{C_0}^2. \quad (5)$$

¹ Note that our observations include data at time $t = 0$. Because the prior is Gaussian and the observational noise is Gaussian we could alternatively redefine the prior to incorporate this data point, which can be done in closed form, and redefine the prior; the observations would then start at time $t = h$.

299 We let $\tilde{m}_0 = \operatorname{argmin}_u I(u)$, that is \tilde{m}_0 returns the value of u at which $I(u)$ achieves its mini-
300 mum. This so-called MAP estimator is, of course, simply the solution of the 4DVAR strong
301 constraint variational method. The mathematical formulation of various inverse problems
302 for the Navier-Stokes equations, justifying the formal manipulations in this subsection, may
303 be found in Cotter et al. (2009).

304 2) FILTERING

305 The posterior filtering distribution at time j given all observations up to time j can also
306 be given in closed form by an application of Bayes' rule. The prior is taken as the predicting
307 distribution:

$$\begin{aligned} \mu_{j|j-1}(u_j) &= \int_{\mathcal{H}} \mathbb{P}(u_j|u_{j-1})\mu_{j-1|j-1}(du_{j-1}) \\ &= \int_{\mathcal{H}} \delta(u_j - \Psi(u_{j-1}))\mu_{j-1|j-1}(du_{j-1}). \end{aligned} \quad (6)$$

308 The δ function appears because the dynamical model is deterministic. As we did for smooth-
309 ing, we can apply Bayes rule to obtain the ratio of the density of $\mu_{j|j}$ with respect to $\mu_{j|j-1}$
310 to obtain

$$\frac{\mu_{j|j}(u)}{\mu_{j|j-1}(u)} \propto \exp\{-\Phi_j(u)\}, \quad (7)$$

312 where

$$\Phi_j(u) = \frac{1}{2} \|y_j - u\|_{\Gamma}^2. \quad (8)$$

314 Together (6) and (7) provide an iteration which, at the final observation time, yields
315 the measure $\mu_{J|J}$. As mentioned in the introduction, this distribution can be obtained by
316 evolving the posterior smoothing distribution $\mu_{0|J}$ forward in time under the dynamics given
317 by (2).

3. Overview of Methods

In this section, we provide details of the various computational methods we use to obtain information about the probability distribution on the state of the system, given observations, in both the smoothing and filtering contexts. To approximate the gold standard, the Bayesian posterior distribution, we use state-of-the-art Markov chain Monte Carlo (MCMC) sampling for the inverse problem, to obtain a large number of samples from the posterior distribution, sufficient to represent its mode and the posterior spread around it. We also describe optimization techniques to compute the MAP estimator of the posterior density, namely 4DVAR. Both the Bayesian posterior sampling and 4DVAR are based on obtaining information from the smoothing distribution from subsection 1. Then we describe a variety of filters, all building on the description of sequential filtering distributions introduced in subsection 2, using Gaussian approximations of one form or another. These filters are 3DVAR, the Fourier Diagonal Filter, the Extended Kalman filter, and the Ensemble Kalman filter. We will refer to these filtering algorithms collectively as *approximate Gaussian filters* to highlight the fact that they are all derived by imposing a Gaussian approximation in the prediction step.

a. MCMC Sampling of the Posterior

We work in the setting of the Metropolis-Hastings variant of MCMC methods, employing recently developed methods which scale well with respect to system dimension; see Cotter et al. (2011) for further details and references. The resulting random walk method that we use to sample from $\mu_{0|J}$ is given as follows²:

- Draw $u^{(0)} \sim \mathcal{N}(m_0, \mathcal{C}_0)$ and set $n = 1$.
- Define $m^* = \sqrt{1 - \beta^2}u^{(n-1)} + (1 - \sqrt{1 - \beta^2})m_0$.

²w.p. denotes “with probability”

- Draw

$$u^* \sim \mathcal{N}(m^*, \beta^2 \mathcal{C}_0),$$

- 341 • Let $\alpha^{(n-1)} = \min\{1, \exp(\Phi(u^{(n-1)}) - \Phi(u^*))\}$ and set

$$u^{(n)} = \left\{ \begin{array}{ll} u^* & \text{w.p. } \alpha^{(n-1)} \\ u^{(n-1)} & \text{else.} \end{array} \right\}$$

- 342 • $n \mapsto n + 1$ and repeat.

343 After a burn-in period of M steps, $\{u^{(n)}\}_{n=M}^N \sim \mu_{0|J}$. This sample is then pushed forward
 344 to yield a sample of time-dependent solutions, $\{u^{(n)}(t)\}$, where $u^{(n)}(t) = \Psi(u^{(n)}; t)$, or in
 345 particular in what follows, a sample of the filtering distribution $\{\Psi^J u^{(n)}\}$.

346 *b. Variational Methods: 4DVAR*

347 As described in section 2, the minimizer of I defined in Eq. (5) defines the 4DVAR
 348 approximation, the basic variational method. A variety of optimization routines can be
 349 used to solve this problem. We have found Newton's method to be effective, with an initial
 350 starting point computed by homotopy methods starting from an easily computable problem.

We now outline how the 4DVAR solution may be used to generate an approximation to the distribution of interest. The 4DVAR solution (MAP estimator) coincides with the mean for unimodal symmetric distributions. If the variance under $\mu_{0|J}$ is small then it is natural to seek a Gaussian approximation. This has the form $\mathcal{N}(\tilde{m}_0, \tilde{\mathcal{C}}_0)$ where

$$\tilde{\mathcal{C}}_0^{-1} = D^2 I(\tilde{m}_0) = D^2 \Phi(\tilde{m}_0) + \mathcal{C}_0^{-1}.$$

Here D^2 denotes the second derivative operator. This Gaussian on the initial condition u_0 can be mapped forward under the dynamics, using linearization for the covariance, since it is assumed small, to obtain $u(t) \approx \mathcal{N}(\tilde{m}(t), \tilde{\mathcal{C}}(t))$ where $\tilde{m}(t) = \Psi(\tilde{m}_0; t)$ and

$$\tilde{\mathcal{C}}(t) = D\Psi(\tilde{m}_0; t)\tilde{\mathcal{C}}_0 D\Psi(\tilde{m}_0; t)^*.$$

351 Here D denotes the derivative operator, and $*$ the adjoint.

353 Recall the key update formulae (6), (7). Note that the integrals are over the function space
 354 \mathcal{H} , a fact which points to the extreme computational complexity of characterizing probability
 355 distributions for problems arising from PDEs or their high dimensional approximation. We
 356 will describe various approximations, which are all Gaussian in nature, and make the update
 357 formulae tractable. We describe some generalities relating to this issue, before describing
 358 various method dependent specifics in following subsections.

359 If Ψ is nonlinear then $\mu_{j-1|j-1}$ Gaussian does not imply $\mu_{j|j-1}$ is Gaussian; this follows
 360 from (6). Thus prediction cannot be performed simply by mapping mean and covariance.
 361 However, the update equation (7) has the property that, if $\mu_{j|j-1}$ is Gaussian then so is $\mu_{j|j}$.
 362 If we assume that $\mu_{j|j-1} = \mathcal{N}(m_j, \mathcal{C}_j)$, then (7) shows that $\mu_{j|j}$ is Gaussian $\mathcal{N}(\hat{m}_j, \hat{\mathcal{C}}_j)$ where
 363 \hat{m}_j is the MAP estimator given by

$$364 \quad \hat{m}_j = \underset{u}{\operatorname{argmin}} I_j(u), \quad (9)$$

(so that \hat{m}_j minimizes $I_j(u)$) and

$$I_j(u) = \Phi_j(u) + \frac{1}{2} \|u - m_j\|_{\mathcal{C}_j}^2.$$

365 Note that, using (8), we see that I_j is a quadratic form whose minimizer is given in closed
 366 form as the solution of a linear equation with the form

$$367 \quad \hat{m}_j = \hat{\mathcal{C}}_j \left(\mathcal{C}_j^{-1} m_j + \Gamma^{-1} y_j \right) \quad (10)$$

368 where

$$369 \quad \hat{\mathcal{C}}_j^{-1} = \mathcal{C}_j^{-1} + \Gamma^{-1}. \quad (11)$$

If the output of the prediction step given by (6) is approximated by a Gaussian then this
 provides the basis for a sequential Gaussian approximation method. To be precise, if we
 have that

$$\mu_{j-1|j-1} = \mathcal{N}(\hat{m}_{j-1}, \hat{\mathcal{C}}_{j-1})$$

370 and we have formulae, based on an approximation of (6), which enable us to compute the
 371 map

$$372 \quad (\hat{m}_{j-1}, \hat{\mathcal{C}}_{j-1}) \mapsto (m_j, \mathcal{C}_j) \quad (12)$$

373 then together (10), (11), (12) provide an iteration for Gaussian approximations of the filtering
 374 distribution $\mu_{j|j}$ of the form

$$375 \quad (\hat{m}_{j-1}, \hat{\mathcal{C}}_{j-1}) \mapsto (\hat{m}_j, \hat{\mathcal{C}}_j).$$

376 In the next few subsections we explain a variety of such approximations, and the resulting
 377 filters.

378 1) CONSTANT GAUSSIAN FILTER (3DVAR)

379 The constant Gaussian filter, referred to as 3DVAR, consists of making the choices $m_j =$
 380 $\Psi(\hat{m}_{j-1})$ and $\mathcal{C}_j \equiv \mathcal{C}$ in (12). It is natural, theoretically, to choose $\mathcal{C} = \mathcal{C}_0$ the prior covariance
 381 on the initial condition. However, as we will see, other issues may intervene and suggest or
 382 necessitate other choices.

383 2) FOURIER DIAGONAL FILTER (FDF)

384 A first step beyond 3DVAR, which employs constant covariances when updating to incor-
 385 porate new data, is to use some approximate dynamics in order to make the update (12). In
 386 Harlim and Majda (2008); Majda et al. (2010) it is demonstrated that, in regimes exhibiting
 387 chaotic dynamics, linear stochastic models can be quite effective for this purpose: this is the
 388 idea of the Fourier Diagonal Filter. In this subsection we describe how this idea may be used,
 389 in both the steady and trubulent regimes of the Navier-Stokes system under consideration.
 390 For our purposes, and as observed in Harlim and Majda (2008), this approach provides a
 391 rational way of deriving the covariances in 3DVAR, based on climatological statistics.

392 The basic idea is, for the purposes of filtering, to replace the nonlinear map $u_{j+1} = \Psi(u_j)$

393 by the linear (stochastic when $\mathcal{Q} \neq 0$) map

$$394 \quad u_{j+1} = Lu_j + \sqrt{\mathcal{Q}}\xi_j. \quad (13)$$

395 Here it is assumed that L is negative definite and diagonal in the Fourier basis, \mathcal{Q} has
 396 summable eigenvalues and is diagonal in the Fourier basis and ξ_j is a random noise chosen
 397 from the distribution $\mathcal{N}(0, I)$. More sophisticated linear stochastic models could (and should)
 398 be used, but we employ this simplest of models to convey our ideas.

399 If $L = \exp(-Mh)$ and $\mathcal{Q} = [I - \exp(-2Mh)]\Xi$, then (13) corresponds to the discrete
 400 time h solution of the Ornstein-Uhlenbeck (OU) process

$$401 \quad du + Mudt = \sqrt{2M\Xi}dW,$$

402 where dW is the infinitesimal Brownian motion increment with identity covariance. The
 403 stationary solution is $\mathcal{N}(0, \Xi)$ and letting $M_{k,k} = \alpha_k$, the correlation time for mode k can
 404 be computed as $1/\alpha_k$. We employ three models of the form (13) in this paper, labelled a),
 405 b) and c), and detailed below. Before turning to them, we describe how this linear model is
 406 incorporated into the filter.

In the case of linear dynamics such as these, the map (12) is given in closed form

$$m_j = L\hat{m}_{j-1}, \quad \mathcal{C}_j = L\hat{\mathcal{C}}_{j-1}L^* + \mathcal{Q}.$$

407 This can be improved, however, in the spirit of 3DVAR, by updating only the covariance in
 408 this way and mapping the mean under the nonlinear map, to obtain the following instance
 409 of (12):

$$410 \quad m_j = \Psi(\hat{m}_{j-1}), \quad \mathcal{C}_j = L\hat{\mathcal{C}}_{j-1}L^* + \mathcal{Q}.$$

411 We implement the method in this form. We note that, because L is negative-definite, the
 412 covariance \mathcal{C}_j converges to some \mathcal{C}_∞ which can be computed explicitly, and, asymptotically,
 413 the algorithm behaves like 3DVAR with a systematic choice of covariance. We now turn to
 414 the choices of L and \mathcal{Q} .

415 **Model (a)** is used in the stationary regime. It is found by setting $L = \exp(-\nu Ah)$
 416 and taking $\mathcal{Q} = \epsilon I$ where $\epsilon = 10^{-12}$. Although this does not correspond to an accurate
 417 linearization of the model in low wave numbers, it is reasonable for high wave numbers.

Model (b) is used in the strongly chaotic regime, and is based on the original idea in Harlim and Majda (2008); Majda et al. (2010). The two quantities $\Xi_{k,k}$ and α_k are matched to the statistics of the dynamical model, as follows. Let $u(t)$ denote the solution to the Navier-Stokes equation (1) which, abusing notation, we assume to be represented in the Fourier domain, with entries $u_k(t)$. Then \bar{u} and Ξ are given by the formulae

$$\bar{u} = \lim_{T \rightarrow \infty} \frac{1}{T} \int_0^T u(t) dt,$$

$$\Xi = \lim_{T \rightarrow \infty} \frac{1}{T} \int_0^T (u(t) - \bar{u}) \otimes (u(t) - \bar{u})^* dt.$$

418 In practice these integrals are approximated by finite discrete sums. Furthermore, we set
 419 the off-diagonal entries of Ξ to zero to obtain a diagonal model. We set $\sigma_k^2 = \Xi_{k,k}$. Then the
 420 α_k are computed using the formulae

$$M(t, \tau) = (u(t - \tau) - \bar{u}) \otimes (u(t) - \bar{u})^*$$

$$\text{Corr}_k(\tau) = \lim_{T \rightarrow \infty} \frac{1}{\sigma_k^2} \int_0^T M_{k,k}(t, \tau) dt$$

$$\alpha_k = \left(\int_0^\infty \text{Re}(\text{Corr}_k(\tau)) d\tau \right)^{-1}.$$

421 Again, finite discrete sums are used to approximate the integrals.

422 3) LOW RANK EXTENDED KALMAN FILTER (LREXKF)

423 The idea of the extended Kalman filter is to assume that the desired distributions are
 424 approximately Gaussian with small covariance. Then linearization may be used to show that

425 a natural approximation of (12) is the map ³

$$426 \quad m_j = \Psi(\hat{m}_{j-1}), \quad \mathcal{C}_j = D\Psi(\hat{m}_{j-1})\hat{\mathcal{C}}_{j-1}D\Psi(\hat{m}_{j-1})^*. \quad (14)$$

427 Updating the covariance this way requires one forward tangent linear solve and one adjoint
428 solve for each dimension of the system, and is therefore prohibitively expensive for high
429 dimensional problems. To overcome this we use a low rank approximation to the covariance
430 update.

We write this explicitly as follows. Compute the dominant m eigenpairs of \mathcal{C}_j as defined
in Eq. (14); these satisfy

$$D\Psi(\hat{m}_{j-1})\hat{\mathcal{C}}_{j-1}D\Psi(\hat{m}_{j-1})^*V = V\Lambda$$

431 Define the rank m matrix $\mathcal{M} = V\Lambda V^*$ and note that this captures the essence of the
432 covariance implied by the extended Kalman filter, in the directions of the m dominant
433 eigenpairs. When the eigenvalues are well-separated, as they are here, a small number of
434 eigenvalues capture the majority of the action and this is very efficient. We then implement
435 the filter

$$436 \quad m_j = \Psi(\hat{m}_{j-1}), \quad \mathcal{C}_j = \mathcal{M} + \epsilon I \quad (15)$$

437 where $\epsilon = 10^{-12}$ as above. The perturbation term prevents degeneracy.

438 The notion of keeping track of the unstable directions of the dynamical model is not new,
439 although our particular implementation differs in some details. For discussions and examples
440 of this idea see Toth and Kalnay (1997), Palmer et al. (1998), Kalnay (2003), Leutbecher
441 (2003), Auvinen et al. (2009), and Hamill et al. (2000).

³As an aside, we note a more sophisticated improved version we have not seen yet in the literature would include the higher-order drift term involving the Hessian. Although adding significant expense there could be scenarios in which this is worthwhile to attempt this.

442 4) ENSEMBLE KALMAN FILTER (ENKF)

443 The Ensemble Kalman Filter, introduced in Evensen et al. (1994) and overviewed in
 444 Evensen (2003, 2009), is slightly outside the framework of the previous three filters and there
 445 are many versions (see Lei et al. (2010) for a comparison between two major categories.) This
 446 is because the basic object which is updated is an ensemble of particles, not a mean and
 447 covariance. This ensemble is used to compute an empirical mean and covariance. We
 448 describe how the basic building blocks of approximate Gaussian filters, namely (10), (11)
 449 and (12), are modified to use ensemble statistics.

We start with (12). Assuming one has an ensemble $\{\hat{m}_{j-1}^{(n)}\} \sim \mathcal{N}(\hat{m}_{j-1}, \hat{\mathcal{C}}_{j-1})$, (12) is replaced by the approximations

$$m_j^{(n)} = \Psi(\hat{m}_{j-1}^{(n)})$$

$$m_j = \frac{1}{N} \sum_{n=1}^N m_j^{(n)}$$

450 and

$$451 \quad \mathcal{C}_j = \frac{1}{N} \sum_{n=1}^N (m_j^{(n)} - m_j)(m_j^{(n)} - m_j)^*. \quad (16)$$

452 The equation (10) is approximated via an ensemble of equations found by replacing m_j by
 453 $m_j^{(n)}$ and replacing y_j by independent draws $\{y_j^{(n)}\}$ from $\mathcal{N}(y_j, \Gamma)$. This leads to updates of
 454 the ensemble members $m_j^{(n)} \mapsto \hat{m}_j^{(n)}$ whose sample mean yields \hat{m}_j . For infinite particles,
 455 the sample covariance yields $\hat{\mathcal{C}}_j$. In the comparisons we consider the covariance to be the
 456 analytical one $\hat{\mathcal{C}}_j = (I - \mathcal{C}_{j-1}(\mathcal{C}_{j-1} + \Gamma)^{-1})\mathcal{C}_{j-1}$ as in (11), rather than the ensemble sample
 457 covariance, which yields the one implicitly in the next update (12). The discrepancy between
 458 these can be large for small samples and in different situations it may have either a positive
 459 or negative effect on the filter divergence discussed in Section 5. Solutions of the ensemble of
 460 equations of form (10) are implemented in the standard Kalman filter fashion; this does not
 461 involve computing the inverse covariances which appear in (11). There are many variants
 462 on the EnKF and we have simply chosen one representative version. See, for example,
 463 Tippett et al. (2003) and Evensen (2009).

4. Filter Accuracy

In this section we describe various aspects of the accuracy of both variational methods (4DVAR) and approximate Gaussian filters, evaluating them with respect to their effectiveness in reproducing the following two quantities: (i) the posterior distribution on state given observations; (ii) the truth u^\dagger which gives rise to the observations. The first of these is found by means of accurate MCMC simulations, and is then characterized by three quantities: its mean, variance, and MAP estimator. It is our contention that, where quantification of uncertainty is important, the comparison of algorithms by their ability to predict (i) is central; however many algorithms are benchmarked in the literature by their ability to predict the truth (ii) and so we also include this information. A comparison of the algorithms with (iii) the observational data is also included as a useful check on the performance of the algorithms. Note that studying the error in (i) requires comparison of probability distributions; we do this primarily through comparison of mean and covariance information. In all our simulations the posterior distribution, and the distributions implied by the variational and filtering algorithms, are approximately Gaussian; for this reason studying the mean and covariance is sufficient. We note that we have not included model error in our study: uncertainty in the dynamical model comes only through the initial condition; thus attempting to match the “truth” is not unnatural in our setting. Matching the posterior distribution is, however, arguably more natural and is a concept which generalizes in a straightforward fashion to the inclusion of model error. In this section all methods are presented in their “raw” form, unmodified and not optimized. Modifications that are often used in practice are discussed in the next section.

a. Nature of Approximations

In this preliminary discussion we make *three observations* which help to guide and understand subsequent numerical experiments. For the purposes of this discussion we assume

489 that the MCMC method, our gold standard, provides *exact* samples from the desired poste-
490 rior distribution. There are then two key approximations underlying the methods which we
491 benchmark against MCMC in this section. The first is the Gaussian approximation, which
492 is made in 3DVAR/FDF, 4DVAR (when propagating from $t = 0$ to $t = T$), LRExKF and
493 EnKF; the second additional approximation is sampling, which is made only in EnKF. The
494 3DVAR and FDF methods make a universal, steady approximation to the covariance whilst
495 4DVAR, LRExKF and EnKF all propagate the approximate covariance using the dynamical
496 model. Our first observation is thus that *we expect 3DVAR and FDF to underperform the*
497 *other methods with regard to covariance information.* The second observation arises from
498 the following: the predicting (and hence smoothing and filtering) distribution will remain
499 close to Gaussian as long as there is a balance between dynamics remaining close to linear
500 and the covariance being small enough (i.e. there is an appropriate level of either of these
501 factors which can counteract any instance of the other one). In this case the evolution of
502 the distribution is well approximated to leading order by the non-autonomous linear system
503 update of ExKF, and similarly for the 4DVAR update from $t = 0$ to $t = T$. Our second
504 observation is hence that *the bias in the Gaussian approximation will become significant if*
505 *the dynamics is sufficiently non-linear or if the covariance becomes large enough.* These two
506 factors which destroy the Gaussian approximation will be more pronounced as the Reynolds
507 number increases, leading to more, and larger, growing (local) Lyapunov exponents, and as
508 the time interval between observations increases, allowing further growth or, for 4DVAR,
509 as the total time-interval grows. The third and final observation concerns EnKF methods.
510 In addition to making the Gaussian approximation, these rely on sampling to capture the
511 resulting Gaussian. Hence the error in the EnKF methods will become significant if the
512 number of samples is too small, even when the Gaussian approximation is valid. Further-
513 more, since the number of samples required tends to grow with both dimension and with
514 the inverse of the size of the quantity being measured, we expect that EnKF will encounter
515 difficulties in this high dimensional system which will be exacerbated when the covariance

516 is small.

517 We will show in the following that in the stationary case, and for high frequency obser-
518 vations in the strongly chaotic case, the ExKF does perform well because of an appropriate
519 balance of the level of nonlinearity of the dynamics on the scale of the time between obser-
520 vations and the magnitude of the covariance. Nonetheless, a reasonable sized ensemble in
521 the EnKF is not sufficiently large for the error from that algorithm to be dominated by the
522 ExKF error, and it is instead determined by the error in the sample statistics with which
523 EnKF approximates the mean and covariance; this latter effect was demonstrated on a sim-
524 pler model problem in Apte et al. (2008b). When the observations are sufficiently sparse in
525 time in the strongly chaotic case the Gaussian approximation is no longer valid and even the
526 ExKF fails to recover accurate mean and covariance.

527 *b. Illustration via Two Regimes*

528 This section is divided into two subsections, each devoted to a dynamical regime: sta-
529 tionary, and strongly chaotic. The true initial condition u^\dagger in the case of strongly chaotic
530 dynamics is taken as an arbitrary point on the attractor obtained by simulating an arbitrary
531 initial condition until statistical equilibrium. The initial condition for the case of stationary
532 dynamics is taken as a draw from the Gaussian prior, since the statistical equilibrium is the
533 trivial one. Note that in the stationary dynamical regime the equation is dominated by the
534 linear term and hence this regime acts as a benchmark for the approximate Kalman filters,
535 since they are exact in the linear case. Each of these sections in turn explores the particular
536 characteristics of the filter accuracy inherent to that regime as a function of time between
537 observations, h . The final time, T , will mostly be fixed, so that decreasing h will increase
538 the density of observations of the system on a fixed time domain; however, on several occa-
539 sions we study the effect of fixing h and changing the final time T . Studies of the effect on
540 the posterior distribution of increasing the number of observations are undertaken for some
541 simple inverse problems in fluid mechanics in Cotter et al. (2011) and are not undertaken

542 here.

We now explain the basic format of the tables which follow and indicate the major features of the filters that they exhibit. The first 8 rows each correspond to a *method* of assimilation, while the final two rows correspond to the truth, at the start and end of the time window studied, for completeness. Labels for these rows are given in the far left column. The posterior distribution (MCMC) and MAP estimator (4DVAR) are each obtained via the smoothing distribution, and hence comparison is made at the initial time, $t = 0$, and at the final time, $t = T$, by mapping forward. For all other methods, the comparison is only with the filtering distribution at the final time, $t = T$. The columns each indicate the relative error of the given filter with a particular diagnostic quantity of interest. The first, third, fourth and fifth columns show $e = \|M(t) - m(t)\|/\|M(t)\|$, where M is, respectively, the mean of the posterior distribution found by MCMC and denoted $\mathbb{E}u(t)$, the truth $u^\dagger(t)$, the observation $y(t)$, or the MAP estimator (4DVAR) at time t (either 0 or T) and $m(t)$ is the time t mean of the filtering (or smoothing) distribution obtained from each of the various methods. The norm used is the $L^2([-1, 1] \times [-1, 1])$ norm. The second column shows

$$e = \frac{\|\text{var}(u(t)) - \text{var}(U(t))\|}{\|\text{var}(u(t))\|}$$

543 where var indicates the variance, u is sampled from the posterior distribution (via MCMC),
544 and U is the Gaussian approximate state obtained from the various methods. The subscripts
545 in the titles in the top row indicate which relative error is given in that column.

546 The following universal observations can be made independent of model parametric
547 regime.

- 548 • The numerical results support the three observations made in the previous subsection.
- 549 • Most algorithms do a reasonably good job of reproducing the mean of the posterior
550 distribution.
- 551 • The LRExKF and 4DVAR both do a reasonably good job of reproducing the variance
552 of the posterior distribution if the Reynolds number is sufficiently small and/or the

553 observation frequency high; otherwise there are circumstances where the approxima-
554 tions underlying the ad hoc filters are not justified and they then fail to reproduce
555 covariance information with any accuracy.

556 • All other algorithms perform poorly when reproducing the variance of the posterior
557 distribution.

558 • All estimators of the mean are uniformly closer to the truth than the observations for
559 all h .

560 • In almost all cases, the estimators of the mean are closer to the mean of the posterior
561 distribution than to the truth.

562 • The error of the estimators of the mean with respect to the truth tends to increase
563 with increasing h .

564 • The error of the mean with respect to the truth decreases for increasing number of
565 observations.

566 • LRExKF usually has the smallest error with respect to the posterior mean and some-
567 times accurately recovers the variance.

568 • The error in the variance is sometimes overestimated and sometimes underestimated,
569 and usually this is wavenumber-dependent in the sense that the variance of certain
570 modes is overestimated and the variance of others is under-estimated. This will be
571 discussed further in the next section.

572 • The posterior smoothing distribution becomes noticeably non-Gaussian although still
573 unimodal, while the filtering distribution remains very close to Gaussian.

575 In the stationary regime, $\nu = 0.1$, the basic time-step used is $dt = 0.05$, the smallest h
576 considered is $h = 0.2$, and we fix $T = 2$ as the filtering time at which to make comparisons
577 of the approximate filters with the moments of the posterior distribution via samples from
578 MCMC, the MAP estimator from 4DVAR, the truth, and the observations. Figure 1 shows
579 the vorticity, w (left), and Fourier coefficients, $|u_k|$ (right), of the smoothing distribution at
580 $t = 0$ in the case that $h = 0.2$. The top panels are the mean of the posterior distribution
581 found with MCMC, $(\mathbb{E}u)$, and the bottom panels are the truth, $u^\dagger(0)$. The MAP estimator
582 (minimizer of $I(u)$, $\hat{m}_0 = \operatorname{argmin} I$) is not shown because it is not discernable from the mean
583 in this case. Notice that the mean (and MAP estimator) on the initial condition resemble
584 the large-scale structure of the truth, but are more rough. This roughness is caused by
585 the presence of the prior mean m_0 drawn according to the distribution $\mathcal{N}(u^\dagger(0), \mathcal{C}_0)$. The
586 solution operator Ψ immediately removes this roughness as it damps high wavenumbers; this
587 effect can be seen in the images of the smoothing distribution mapped forward to time $t = T$,
588 i.e. the filtering distribution, in Figure 2 (here only the mean is shown, as neither the truth
589 nor the MAP estimator are distinguishable from it). This is apparent in the data in the
590 tables discussed below, in which the distance between the truth, the posterior distribution,
591 and the MAP estimator are all mutually much closer for the final time than the initial;
592 this contraction of the errors in time is caused by the underlying dynamics which involves
593 exponential attraction to a unique stationary state. This is further exhibited in Figure 3
594 which shows the histogram of the smoothing distribution for the real part of a sample mode,
595 $u_{1,1}$, at the initial time (left) and final time (right).

596 Table 1 presents data for increasing $h = 0.2, 1, 2$, with $T = 2$ fixed. Notable trends,
597 in addition to those mentioned at the start of this section, are as follows: (i) the 4DVAR
598 smoothing distribution has much smaller error with respect to the mean at $t = T$ than at
599 $t = 0$, with the former increasing and the latter decreasing for increasing h ; the error of
600 4DVAR with respect to the mean and the variance at $t = 0$ and $t = T$ are close to or below

601 the threshold of accuracy of MCMC; (iii) the error of both the mean and the variance of
 602 3DVAR tend to decrease with increasing h ;

603 *d. Strongly Chaotic Regime*

604 In the strongly chaotic regime, $\nu = 0.01$, the basic time-step used is $dt = 0.005$, the
 605 smallest h considered is $h = 0.02$, and we fix $T = 0.2$ or $T = 1$ as the filtering time at which
 606 to make comparisons of the approximate filters. In this regime, the dynamics are significantly
 607 more nonlinear and less predictable, with a high-dimensional attractor spanning many scales.
 608 Indeed the energy spectrum decays like $E(k) = \lim_{\delta \rightarrow 0} \int_0^{2\pi} \int_k^{k+\delta} \mathbb{E}|u_l|^2 l dl d\theta \propto k^{-2/3}$ for
 609 $|k| < k_f$, with k_f the magnitude of the forcing wavenumber, and much more rapidly for
 610 $|k| > k_f$. See the left panel of Figure 4 for the average spectrum of the solution on the
 611 attractor and Fig. 5 for an example snapshot of the solution on the attractor. The flow
 612 is not in any of the classical regimes of cascades, but there is an upscale transfer of energy
 613 because of the forcing at intermediate scale. The viscosity is not negligible even at the largest
 614 scales, thereby allowing statistical equilibrium; this may be thought of as being generated
 615 by the empirical measure on the global attractor whose existence is assured for all $\nu > 0$.
 616 We confirmed this with simulations to times of order $O(10^3\nu)$ giving $O(10^7)$ samples with
 617 which to compute the converged correlation statistics used in FDF.

618 Small perturbations in the directions of maximal growth of the dynamics grow substan-
 619 tially over the larger times between observations we look at, while over the shorter times the
 620 dynamics remain well approximated by the linearization. See the right panel of Figure 4 for
 621 an example of the local maximal growth of perturbations. Figure 5 shows the initial and final
 622 time profiles of the mean as in Figures 1 and 2. Now that the solutions themselves are more
 623 rough, it is not possible to notice the influence of the prior mean at $t = 0$, and the profiles
 624 of the truth and MAP are indistinguishable from the mean throughout the interval of time.
 625 The situation in this regime is significantly different from the situation close to a stationary
 626 solution, primarily because the dimension of the attractor is very large and the dynamics on

627 it are very unpredictable. Notice in Figure 6 (top) that the uncertainty in u_{11} now barely
 628 decreases as we pass from initial time $t = 0$ to final time $t = T$. Indeed for moderately high
 629 modes, the uncertainty increases (see 6 (bottom) for the distribution of u_{55}).

630 Table 2 presents data for increasing $h = 0.02, 0.1, 0.2$, with $T = 0.2$ fixed. Table 3
 631 shows data for increasing $h = 0.2, 0.5$ with $T = 1$ fixed. Notable trends, in addition to
 632 those mentioned at the start of the section, are: (i) when computable, the variance of the
 633 4DVAR smoothing distribution has smaller error at $t = 0$ than at $t = T$; (ii) the 4DVAR
 634 smoothing distribution error with respect to the variance cannot be computed accurately
 635 for $T = 1$ because of accumulated error for long times in the approximation of the adjoint of
 636 the forward operator by the discretization of the analytical adjoint; (iii) the error of 4DVAR
 637 with respect to the mean at $t = 0$ for $h \leq 0.1$ is below the threshold of accuracy of MCMC;
 638 (iv) the error in the variance for the FDF algorithm is very large because the \mathcal{Q} is an order
 639 of magnitude larger than Γ ; (v) the FDF algorithm is consistent in recovering the mean for
 640 increasing h , while the other algorithms deteriorate; (vi) the error of FDF with respect to
 641 the variance decreases with increasing h ; (vii) for $h = 0.5$ and $T = 1$ the FDF performs best
 642 and these desirable properties of the FDF variant on 3DVAR are associated with stability
 643 and will be discussed in the next section; (viii) for increasing h , the error in the mean of
 644 LRExKF increases first when $h = 0.1$ and $T = 0.2$ and becomes close to the error in the
 645 variance which can be explained by the bias induced by neglecting the next order of the
 646 expansion of the dynamics; (ix) the error in LRExKF is substantial when $T = 1$ and it really
 647 majorly fails when $h = 0.5$ which is consistent with the time-scale on which nonlinear effects
 648 become prominent (see Fig. 4) and the linear approximation would not be expected to be
 649 valid. The error in the mean is larger, again as expected from the Ito correction term.

5. Filter Stability

Many of the accuracy results for the filters described in the previous section are degraded if, as is common practice in applied scenarios, modifications are made to ensure that the algorithms remain stable over longer time-intervals; that is if some form of variance inflation is performed to keep the algorithm close to the true signal, or to prevent it from suffering filter divergence (see Jazwinski (1970), Fisher et al. (2005), Evensen (2009), and references therein). In this section we describe some of the mathematics which underlies stabilization, describe numerical results illustrating it, and investigate its effect on filter accuracy. *The basic conclusion of this section is that stabilization via variance inflation enables algorithms to be run for longer time windows before diverging, but may cause poorer accuracy in both the mean (before divergence) and the variance predictions.* Again, we make no claims of optimal implementation of these filters, but rather aim to describe the mechanism of stabilization and the common effect, in general, as measured by ability to reproduce the gold standard posterior distribution.

We define stability in this context to mean that the distance between the truth and the estimated mean remains small. As we will demonstrate, whether or not this distance remains small depends on whether the observations made are sufficient to control any instabilities inherent in the model dynamics. To understand this issue it is instructive to consider the 3DVAR, FDF and LRExKF filters, all of which use a prediction step (12) which updates the mean using $m_j = \Psi(\hat{m}_{j-1})$. When combined with the data incorporation step (10) we get an update equation of the form

$$\hat{m}_{j+1} = (I - K_j)\Psi(\hat{m}_j) + K_j y_{j+1}, \quad (17)$$

where $K_j = (\mathcal{C}_j^{-1} + \Gamma^{-1})^{-1}\Gamma^{-1}$ is the Kalman gain matrix. If we assume that the data is derived from a true signal u_j^\dagger satisfying $u_{j+1}^\dagger = \Psi(u_j^\dagger)$ and that

$$y_{j+1} = u_{j+1}^\dagger + \eta_j = \Psi(u_j^\dagger) + \eta_j,$$

672 where the η_j denote the observation errors, then we see that (17) has the form

$$673 \quad \hat{m}_{j+1} = (I - K_j)\Psi(\hat{m}_j) + K_j\Psi(u_j^\dagger) + K_j\eta_{j+1}. \quad (18)$$

674 If the observational noise is assumed to be consistent with the model used for the assimilation,
 675 then $\eta_j \sim \mathcal{N}(0, \Gamma)$ are i.i.d. random variables and we note that (18) is an inhomogenous
 676 Markov chain.

677 Note that

$$678 \quad u_{j+1}^\dagger = (I - K_j)\Psi(u_j^\dagger) + K_j\Psi(u_j^\dagger) \quad (19)$$

so that defining the error $e_j := \hat{m}_j - u_j^\dagger$ and subtracting (19) from (18) we obtain the equation

$$e_{j+1} \approx (I - K_j)D_j e_j + K_j\eta_{j+1}$$

679 where $D_j = D\Psi(u_j^\dagger)$. The stability of the filter will be governed by families of products of
 680 the form

$$681 \quad \Pi_{j=0}^{k-1}((I - K_j)D_j), \quad k = 1, \dots, J.$$

682 We observe that $I - K_j$ will act to induce stability, as it has norm less than one in appro-
 683 priate spaces; D_j , however, will induce some instability whenever the dynamics themselves
 684 contain unstable growing modes. The balance between these effects – stabilization through
 685 observation and instability in the dynamics – determines whether the overall algorithm is
 686 stable.

687 The operator K_j weights the relative importance of the model and the observations,
 688 according to covariance information. Therefore, this weighting must effectively stabilize the
 689 growing directions in the dynamics. Note that increasing \mathcal{C}_j – *variance inflation* – has the
 690 effect of moving K_j towards the identity, so the mathematical mechanism of controlling
 691 the instability mechanism by variance inflation is elucidated by the discussion above. In
 692 particular, when the assimilation is proceeding in a stable fashion, the modes in which
 693 growing directions have support typically overestimate the variance to induce this stability.
 694 In unstable cases, there are at least some times at which some modes in which growing

695 directions have support *underestimate* the variance, leading to instability of the filter. It is
 696 always the case that the onset of instability occurs when the distance from the estimated
 697 mean to the truth persistently exceeds the estimated standard deviation. In Brett et al.
 698 (2010) we provide the mathematical details and rigorous proofs which underpin the preceding
 699 discussion.

700 In the following, two observations concerning the size of the error are particularly in-
 701 structive. Firstly, using the distribution assumed on the η_j , the following lower bound on
 702 the error is immediate⁴:

$$703 \quad \mathbb{E}\|e_{j+1}\|^2 \geq \mathbb{E}\|K_j\eta_{j+1}\|^2 = \text{tr}(K_j\Gamma K_j^*). \quad (20)$$

704 This implies that the average scale of the error of the filter, with respect to the truth, is set by
 705 the scale of the observation error, and shows that the choice of the covariance updates, and
 706 hence the Kalman gain K_j , will affect the exact size of the average error, on this scale. The
 707 second observation follows from considering the trivial “filter” obtained by setting $K_j \equiv I$,
 708 which corresponds to simply setting $\hat{m}_j = y_j$ so that all weight is placed on the observations.
 709 In this case the average error is equal to

$$710 \quad \mathbb{E}\|e_{j+1}\|^2 = \mathbb{E}\|\eta_{j+1}\|^2 = \text{tr}(\Gamma). \quad (21)$$

711 As we would hope that incorporation of the model itself improves errors we view (21) as
 712 providing an upper bound on any reasonable filter and we will consider the filter “unstable”
 713 if the squared error from the truth exceeds $\text{tr}(\Gamma)$. Thus we use (21) and (20) as guiding
 714 upper and lower bounds when studying the errors in the filter means in what follows.

715 In cases where our basic algorithm is unstable in the sense just defined we will also imple-
 716 ment a stabilized algorithm, by adopting the commonly used practice of variance inflation.
 717 The discussion above demonstrates how this acts to induce stability by causing the K_j to
 718 move closer to the identity. For 3DVAR this is achieved by taking the original \mathcal{C}_0 and re-
 719 defining it via the transformation $\mathcal{C}_0 \rightarrow \frac{1}{\epsilon}\mathcal{C}_0$. In all the numerical computations presented

⁴Here \mathbb{E} denotes expectation with respect to the random variables η_j .

720 in this paper which concern the stabilized version of 3DVAR we take $\epsilon = 0.01$. The FDF(b)
721 algorithm remains stable since it already has an inflated variance via the model error term.
722 For LRExKF we achieve variance inflation by replacing the perturbation term of Equation
723 15 with $(I - VV^*)\tilde{\mathcal{C}}_j(I - VV^*)$, where $\tilde{\mathcal{C}}_j$ is the covariance arising from FDF(b). Finally
724 we discuss stabilization of the EnKF. This is achieved by taking the original \mathcal{C}_j 's given by
725 (16) and redefining them via the transformations $\mathcal{C}_0 \rightarrow \frac{1}{\epsilon}\mathcal{C}_0$, and $\mathcal{C}_j \rightarrow (1 + \epsilon_i)\mathcal{C}_j + \epsilon_p\mathcal{C}_0$
726 with $\epsilon = 10^{-4}$, $\epsilon_i = 0.1$, $\epsilon_p = 0.01$. The parameter ϵ prevents initial divergence, ϵ_i main-
727 tains stability with direct incremental inflation and ϵ_p provides rank correction. This is only
728 one option out of a wide array of possible hueristically derived such transformations. For
729 example, rank correction is often performed by some form of localization which preserves
730 trace and eliminates long-range correlations, while our rank correction preserves long-range
731 correlations and provides trace inflation. The point here is that our transformation captures
732 the essential mechanism of stabilization by inflation which, again, is our objective.

733 We denote the stabilized versions of 3DVAR, LRExKF, and EnKF by [3DVAR], [LRExKF],
734 and [EnKF]. Because FDF itself always remains stable we do not show results for a stabilized
735 version of this algorithm. Note that we use ensembles in EnKF of equal size to the number
736 of approximate eigenvectors in LRExKF, in order to ensure comparable work. This is always
737 100, except for large h , when some of the largest 100 eigenvalues are too close to zero to
738 maintain accuracy, and so fewer eigenvectors are used in LRExKF in these cases. Also, note
739 again that we are looking for general features across methods and are not aiming to optimize
740 the inflation procedure for any particular method.

741 Examples of an unstable instance of 3DVAR and the corresponding stabilized filter,
742 [3DVAR], are depicted in Figures 8 and 9, respectively, with $\nu = 0.01$, $h = 0.2$. In this
743 regime the dynamics are strongly chaotic. The first point to note is that both simulations
744 give rise to an error which exceeds the lower bound (20); and that the unstable algorithm
745 exceeds the desired bound (21), whilst the stabilized algorithm does not; note also that the
746 stabilized algorithm output is plotted over a longer time-interval than the original algorithm.

747 A second noteworthy point relates to the power of using the dynamical model: this is manifest
748 in the bottom right panels of each figure, in which the trajectory of a high wavenumber
749 mode, close to the forcing frequency, is shown. The assimilation performs remarkably well
750 for the trajectory of this wavenumber relative to the observations in the stabilized case,
751 owing to the high weight on the dynamics and stability of the dynamical model for that
752 wavenumber. Examples of an unstable instance of LRExKF and the corresponding stabilized
753 filter, [LRExKF], are depicted in Figures 10 and 11, respectively, with $\nu = 0.01, h = 0.5$.
754 The behaviour illustrated is very similar to that exhibited for 3DVAR and [3DVAR].

755 In the following tables we make a comparison between the original form of the filters and
756 their stabilized forms, using the gold standard Bayesian posterior distribution as the desired
757 outcome. Table 4 shows data for $h = 0.02$ and 0.2 with $T = 0.2$ fixed. Tables 5 and 6 show
758 data for $h = 0.2$ and 0.5 with $T = 1$ fixed. We focus our discussion on the approximation
759 of the mean. It is noteworthy that, on the shorter time horizon $T = 0.2$, the stabilized
760 algorithms are less accurate with respect to the mean than their original counterparts, for
761 both values of observation time h ; this reflects a lack of accuracy caused by inflating the
762 variance. As would be expected, however, this behaviour is reversed on longer time-intervals,
763 as is shown when $T = 1.0$, reflecting enhanced stability caused by inflating the variance. Table
764 5 shows the case $T = 1.0$ with $h = 0.2$, and the stabilized version of 3DVAR outperforms the
765 original version, although the stabilized versions of EnKF and LRExKF are not as accurate
766 as the original version. In Table 6, with $h = 0.5$ and $T = 1.0$, the stabilized versions improve
767 upon the original algorithms in all three cases. Furthermore, in Table 6, we also display the
768 FDF showing that, without any stabilization, this outperforms the other three filters and
769 their stabilized counterparts.

6. Conclusion

Incorporating noisy data into uncertain computational models presents a major challenge in many areas of the physical sciences, and in atmospheric modelling and NWP in particular. Data assimilation algorithms in NWP have had measurable positive impact on forecast skill. Nonetheless, assessing the ability of these algorithms to forecast *uncertainty* is more subtle. It is important to do so, however, especially as prediction is pushed to the limits of its validity in terms of time horizons considered, or physical processes modelled. In this paper we have proposed an approach to the evaluation of the ability of data assimilation algorithms to predict uncertainty. The cornerstone of our approach is to adopt a fully non-Gaussian Bayesian perspective in which the probability distribution of the system state over a time horizon, given data over that time horizon, plays a pivotal role: we contend that algorithms should be evaluated by their ability to reproduce this probability distribution, or important aspects of it, accurately.

In order to make this perspective useful it is necessary to find a model problem which admits complex behaviour reminiscent of atmospheric dynamics, whilst being sufficiently small to allow computation of the Bayesian posterior distribution, so that data assimilation algorithms can be compared against it. Although MCMC sampling of the posterior can, in principle, recover any distribution, it becomes prohibitively expensive for multi-modal distributions, depending on the energy barriers between modes. However for unimodal problems, state-of-the-art sampling techniques allow fully resolved MCMC computations to be undertaken. We have found that the 2D Navier-Stokes equations provide a model for which the posterior distribution may be accurately sampled using MCMC, in regimes where the dynamics is stationary and where it is strongly chaotic. We have confined our attention to strong constraint models, and implemented a range of variational and filtering methods, evaluating them by their ability to reproduce the Bayesian posterior distribution. The set-up is such that the Bayesian posterior is unimodal and approximately Gaussian. Thus the evaluation is undertaken by comparing the mean and covariance structure of the data

797 assimilation algorithms against the actual Bayesian posterior mean and covariance. Simi-
798 lar studies were undertaken in the context of a subsurface geophysical inverse problem in
799 Liu and Oliver (2003), although the conclusions were less definitive. It would be interesting
800 to revisit such subsurface geophysical inverse problems using the state-of-the-art MCMC
801 techniques adopted here, in order to compute the posterior distribution. Moreover it would
802 be interesting to conduct a study, similar to that undertaken here, for models of atmo-
803 spheric dynamics such as Lorenz-96, or a quasi-geostrophic models, which admit baroclinic
804 instabilities.

805 These studies, *under the assumption of a well-defined posterior probability distribution*,
806 lead to four conclusions: (i) most filtering and variational algorithms do a reasonably good
807 job of reproducing the mean; (ii) for most of the filtering and variational algorithms studied
808 and implemented here there are circumstances where the approximations underlying the ad
809 hoc filters are not justified and they then fail to reproduce covariance information with any
810 accuracy (iii) most filtering algorithms exhibit instability on longer time-intervals causing
811 them to lose accuracy in even mean prediction; (iv) filter stabilization, via variance inflation
812 of one sort or the other, ameliorates this instability and can improve long-term accuracy of
813 the filters in predicting the mean, but can reduce the accuracy on short time intervals and
814 of course makes it impossible to predict the covariance. In summary most data assimilation
815 algorithms used in practice should be viewed with caution when using them to make claims
816 concerning uncertainty although, when properly tuned, they will frequently track the signal
817 mean accurately for fairly long time intervals. These conclusions are intrinsic to the algo-
818 rithms, and result from the nature of the approximations made in order to create tractable
819 online algorithms; the basic conclusions are not expected to change by use of different dy-
820 namical models, or by modifying the parameters of those algorithms.

821 Finally we note that we have not addressed in this paper the important but complicated
822 issue of how to choose the prior distribution on the initial condition. We finish with some
823 remarks concerning this. The “accuracy of the spread” of the prior is often monitored in

824 practice with a rank histogram Anderson (1996). This can be computed even in the absence
825 of an ensemble for any method in the class of those discussed here, by partitioning the
826 real line in bins according to the assumed Gaussian prior density. It is important to note
827 that uniform component-wise rank histograms in each direction guarantee that there are no
828 directions in which the variance is consistently underestimated, and this should therefore be
829 sufficient for stability. It is also necessary for the accurate approximation of the Bayesian
830 posterior distribution, but by no means sufficient Hamill et al. (2000). Indeed, one can
831 iteratively compute a constant prior with the cycled 3DVAR algorithm Hamill et al. (2000)
832 such that the estimator from the algorithm will have statistics consistent with the constant
833 prior used in the algorithm. The estimator produced by this algorithm is guaranteed by
834 construction to yield uniform rank histograms of the type described above, and yet the
835 actual prior coming from the posterior at the previous time is not constant, so this cannot
836 be a good approximation of the actual prior. See Fig. 7 for an image of the variance which is
837 consistent with the statistics of the estimator over 100 iterations of 3DVAR with $\nu = 0.01$ and
838 $h = 0.5$, as compared with the prior, posterior, and converged FDF variance at $T = 1$. Notice
839 FDF overestimates in the high-variance directions, and underestimates in the low-variance
840 directions (which correspond in our case to the unstable and stable directions, respectively).
841 The RMSE of 3DVAR with constant converged FDF variance is smaller than with constant
842 variance from converged statistics, and yet the former clearly will yield component-wise rank
843 histograms which appear to always underestimate the “spread” in the low-variance, stable
844 directions, and overestimate in the high-variance, unstable directions. It is also noteworthy
845 that the FDF variance accurately recovers the decay of the posterior variance, but is about
846 an order of magnitude larger. Further investigation of how to initialize statistical forecasting
847 algorithms clearly remains a subject presenting many conceptual and practical challenges.

848 *Acknowledgments.*

849 Both authors are grateful to the referees for numerous suggestions which have improved

850 the presentation of this material; In particular, we thank Chris Snyder. KJHL is grateful to
851 the EPSRC for funding. AMS is grateful to EPSRC, ERC and ONR for funding.

852 **7. Appendix: Some numerical details**

853 Here we provide some details of the numerical algorithms underlying the computations
854 which we present in the main body of the paper. First, we will describe the numerical
855 methods used for the dynamical model. Secondly we study the adjoint solver. Thirdly we
856 discuss various issues related to the resulting optimization problems and large linear systems
857 encountered. Finally we discuss the MCMC method used to compute the gold standard
858 posterior probability distribution.

859 In the *dynamical and observational models* the forcing in Eq. 1 is taken to be $f = \nabla^\perp \psi$,
860 where $\psi = \cos(k \cdot x)$ and $\nabla^\perp = J\nabla$ with J the canonical skew-symmetric matrix, and
861 $k = (1, 1)$ for stationary ($\nu = 0.1$) regime, while $k = (5, 5)$ for the strongly chaotic regime in
862 order to allow an upscale cascade of energy. Furthermore, we set the observational noise to
863 white noise $\Gamma = \gamma^2 I$, where $\gamma = 0.04$ is chosen as 10% of the maximum standard deviation
864 of the strongly chaotic dynamics, and we choose an initial smoothness prior $\mathcal{C}_0 = A^{-2}$,
865 where A is the Stokes operator. We notice that only the observations on the unstable
866 manifold of the underlying solution map need to be assimilated. A similar observation was
867 made in Chorin and Krause (2004) in the context of particle filters. Our choice of prior and
868 observational covariance reflect this in the sense that the ratio of the prior to the observational
869 covariance is larger for smaller wavenumbers (and greater than 1, in particular), in which the
870 unstable manifold has support, while this ratio tends to zero as $|k| \rightarrow \infty$. The initial mean,
871 or background state, is chosen as $m_0 \sim \mathcal{N}(u^\dagger, \mathcal{C}_0)$, where u^\dagger is the true initial condition.
872 In the case of strongly chaotic dynamics it is taken as an arbitrary point on the attractor
873 obtained by simulating an arbitrary initial condition until statistical equilibrium. The initial
874 condition for the case of stationary dynamics is taken as a draw from the Gaussian prior,

875 since the statistical equilibrium is the trivial one.

876 Our numerical method for the dynamical model is based on a Galerkin approximation of
877 the velocity field in a divergence-free Fourier basis. We use a modification of a fourth-order
878 Runge-Kutta method, ETD4RK Cox and Matthews (2002), in which the heat semi-group is
879 used together with Duhamel’s principle to solve exactly for the diffusion term. A spectral
880 Galerkin method Hesthaven et al. (2007) is used in which the convolutions arising from
881 products in the nonlinear term are computed via FFTs. We use a double-sized domain in each
882 dimension, buffered with zeros, resulting in 64^2 grid-point FFTs, and only half the modes are
883 retained when transforming back into spectral space in order to prevent de-aliasing which
884 is avoided as long as fewer than $2/3$ the modes are retained. Data assimilation in practice
885 always contends with poor spatial resolution, particularly in the case of the atmosphere
886 in which there are many billions of degrees of freedom. For us the important resolution
887 consideration is that the unstable modes, which usually have long spatial scales and support
888 in low wave-numbers, are resolved. Therefore, our objective here is not to obtain high spatial-
889 resolution but rather to obtain high temporal-resolution in the sense of reproducibility. We
890 would like the divergence of two close-by trajectories to be dictated by instability in the
891 dynamical model rather than the numerical time-stepping scheme.

892 It is also important that we have accurate *adjoint solvers*, and this is strongly linked
893 to the accuracy of the forward solver. The same time-stepper is used to solve the adjoint
894 equation, with twice the time-step of the forward solve, since the forward solution is re-
895 quired at half-steps in order to implement this method for the non-autonomous adjoint solve.
896 Many issues can arise in the implementation of adjoint, or costate methods Banks (1992);
897 Vogel and Wade (1995) and the practitioner should be aware of these. The easiest way to
898 ensure convergence is to test that the tangent linearized map is indeed the linearization of
899 the solution map and then confirm that the adjoint is the adjoint to a suitable threshold. We
900 have taken the approach of “optimize then discretize” here, and as such our adjoint model
901 is the discretization of the analytical adjoint. This effect becomes apparent in the accuracy

902 of the linearization for longer time intervals, and we are no longer able to compute accurate
903 gradients and Hessians as a result.

904 Regarding *linear algebra and optimization* issues we make the following observations. A
905 Krylov method (GMRES) is used for linear solves in the Newton method for 4DVAR, and
906 the Arnoldi method is used for low-rank covariance approximations in LRExKF and for
907 the filtering time T covariance approximation in 4DVAR. The LRExKF always sufficiently
908 captures more than 99% of the full rank version as measured in Frobenius (matrix l^2) norm.
909 The initial Hessian in 4DVAR and well as the ones occurring within Newton's method are
910 computed by finite difference. Using a gradient flow (preconditioned steepest descent) com-
911 putation, we obtain an approximate minimizer close to the actual minimizer and then a
912 preconditioned Newton-Krylov nonlinear fixed-point solver is used (NSOLI Kelley (2003)).
913 This approach is akin to the Levenburgh-Marquardt algorithm. See Trefethen and Bau
914 (1997) and Saad (1996) for overviews of the linear algebra and Nocedal and Wright (1999)
915 for an overview of optimization. Strong constraint 4DVAR can be computationally challeng-
916 ing and, although we do not do so here, it would be interesting to study weak constraint
917 4DVAR from a related perspective; see Bröcker (2010) for a discussion of weak constraint
918 4DVAR in continuous time. It is useful to employ benchmarks in order to confirm gradients
919 are being computed properly when implementing optimizers, see for example Lawless et al.
920 (2003).

921 Finally, we comment on the *MCMC* computations which, of all the algorithms imple-
922 mented here, lead to the highest computational cost. This, of course, is because it fully
923 resolves the posterior distribution of interest whereas the other algorithms use crude ap-
924 proximations, the consequences of which we study by comparison with accurate MCMC
925 results. Each time-step requires 4 function evaluations, and each function evaluation re-
926 quires 8 FFTs, so it costs 32 FFTs for each time-step. We fix the lengths of paths at 40
927 time-steps for most of the computations, but nonetheless, this is on the order of 1000 FFTs
928 per evaluation of the dynamical model. If a 64^2 FFT takes 1 ms, then this amounts to 1 s

929 per sample. Clearly this is a hurdle as it would take on the order of 10 days to obtain on the
930 order of millions of samples in serial. We overcome this by using the MAP estimator (4DVAR
931 solution) as the initial condition in order to accelerate burn-in, and then run independent
932 batches of 10^4 samples in parallel with independent seeds in the random number generator.
933 We also minimize computational effort within the method by employing the technique of early
934 rejection introduced by Haario (2010) which means that rejection can be detected before the
935 forward computation required for evaluation of Φ reaches the end of the assimilation time
936 window; the computation can then be stopped and hence computational savings made.

937 It is important to recognize that we cannot rely too heavily on results of MCMC with
938 smaller relative norm than 10^{-3} for the mean or 10^{-2} for the variance, because we are
939 bound to $\mathcal{O}(N^{-1/2})$ convergence and it is already prohibitively expensive to get several
940 million samples. More than 10^7 is not tractable. Convergence is measured by a version of
941 MSPRF Brooks and Gelman (1998), $ev_{1:8} = \|\text{var}[u_1(t)] - \text{var}[u_8(t)]\|/\|\text{var}[u_1(t)]\|$, where u_1
942 corresponds to sample statistics with 1 chain and u_8 corresponds to sample statistics over
943 8 chains. We find $ev_{1:8} = \mathcal{O}(10^{-2})$ for $N = 3.2 \times 10^5$ samples in each chain. If we define
944 $em_{1:8} = \|\mathbb{E}[u_1(t)] - \mathbb{E}[u_8(t)]\|/\|\mathbb{E}[u_1(t)]\|$, then we have $em_{1:8} = \mathcal{O}(10^{-3})$.

945

946 REFERENCES

- 947 Anderson, J., 1996: A method for producing and evaluating probabilistic forecasts from
948 ensemble model integrations. *Journal of Climate*, **9** (7), 1518–1530.
- 949 Apte, A., M. Hairer, A. Stuart, and J. Voss, 2007: Sampling the posterior: an approach to
950 non-Gaussian data assimilation. *Physica D*, **230**, 50–64.
- 951 Apte, A., C. Jones, and A. Stuart, 2008a: A Bayesian approach to Lagrangian data assimilation.
952 *Tellus*, **60**, 336–347.

953 Apte, A., C. Jones, A. Stuart, and J. Voss, 2008b: Data assimilation: Mathematical and
954 statistical perspectives. *International Journal for Numerical Methods in Fluids*, **56 (8)**,
955 1033–1046.

956 Arulampalam, M., S. Maskell, N. Gordon, and T. Clapp, 2002: A tutorial on particle filters
957 for online nonlinear/non-gaussian bayesian tracking. *Signal Processing, IEEE Transactions*
958 *on*, **50 (2)**, 174–188.

959 Auvinen, H., J. Bardsley, H. Haario, and T. Kauranne, 2009: Large-scale kalman filtering
960 using the limited memory bfgs method. *Electronic Transactions on Numerical Analysis*,
961 **35**, 217–233.

962 Bain, A. and D. Crisan, 2008: *Fundamentals of stochastic filtering*. Springer Verlag.

963 Banks, H., 1992: Computational issues in parameter estimation and feedback control prob-
964 lems for partial differential equation systems. *Physica D: Nonlinear Phenomena*, **60 (1-4)**,
965 226–238.

966 Banks, H. and K. Kunisch, 1989: *Estimation techniques for distributed parameter systems*.
967 Birkhauser Boston.

968 Bengtsson, T., C. Snyder, and D. Nychka, 2003: Toward a nonlinear ensemble filter for
969 high-dimensional systems. *J. Geophys. Res*, **108 (D24)**, 8775.

970 Bennett, A., 2002: *Inverse Modeling of the ocean and Atmosphere*. Cambridge.

971 Brett, C., A. Lam, K. Law, D. McCormick, M. Scott, and A. Stuart, 2010: Stability of filters
972 for the navier-stokes equation. *preprint*.

973 Bröcker, J., 2010: On variational data assimilation in continuous time. *Quarterly Journal of*
974 *the Royal Meteorological Society*, **136 (652)**, 1906–1919.

975 Brooks, S. and A. Gelman, 1998: General methods for monitoring convergence of iterative
976 simulations. *Journal of Computational and Graphical Statistics*, **7 (4)**, 434–455.

977 Bryson, A. and M. Frazier, 1963: Smoothing for linear and nonlinear dynamic systems.
978 *Proceedings Optimum System Sythensis Conference*, US Air Force Tech. Rep. AFB-TDR-
979 63-119.

- 980 Carrassi, A., M. Ghil, A. Trevisan, and F. Uboldi, 2008: Data assimilation as a nonlin-
981 ear dynamical systems problem: Stability and convergence of the prediction-assimilation
982 system. *Chaos: An Interdisciplinary Journal of Nonlinear Science*, **18**, 023 112.
- 983 Chorin, A. and P. Krause, 2004: Dimensional reduction for a bayesian filter. *Proceedings of*
984 *the National Academy of Sciences of the United States of America*, **101 (42)**, 15 013.
- 985 Chorin, A., M. Morzfeld, and X. Tu, 2010: Implicit particle filters for data assimilation.
986 *Communications in Applied Mathematics and Computational Science*, 221.
- 987 Cotter, S., M. Dashti, J. Robinson, and A. Stuart, 2009: Bayesian inverse problems for
988 functions and applications to fluid mechanics. *Inverse Problems*, **25**, 115 008.
- 989 Cotter, S., M. Dashti, and A. Stuart, 2011: Variational data assimilation using targetted
990 random walks. *Int. J. Num. Meth. Fluids*.
- 991 Courtier, P. and O. Talagrand, 1987: Variational assimilation of meteorological observations
992 with the adjoint vorticity equation. ii: Numerical results. *Quarterly Journal of the Royal*
993 *Meteorological Society*, **113 (478)**, 1329–1347.
- 994 Cox, H., 1964: On the estimation of state variables and parameters for noisy dynamic
995 systems. *Automatic Control, IEEE Transactions on*, **9 (1)**, 5–12.
- 996 Cox, S. and P. Matthews, 2002: Exponential time differencing for stiff systems. *Journal of*
997 *Computational Physics*, **176 (2)**, 430–455.
- 998 Doucet, A., N. De Freitas, and N. Gordon, 2001: *Sequential Monte Carlo methods in practice*.
999 Springer Verlag.
- 1000 Evensen, G., 2003: The ensemble kalman filter: Theoretical formulation and practical im-
1001 plementation. *Ocean dynamics*, **53 (4)**, 343–367.
- 1002 Evensen, G., 2009: *Data assimilation: the ensemble Kalman filter*. Springer Verlag.
- 1003 Evensen, G., P. Van Leeuwen, et al., 1994: Assimilation of geosat altimeter data for the
1004 agulhas current using the ensemble kalman filter with a quasi-geostrophic model. *Monthly*
1005 *Weather*.
- 1006 Fisher, M., M. Leutbecher, and G. Kelly, 2005: On the equivalence between kalman smooth-

1007 ing and weak-constraint four-dimensional variational data assimilation. *Quarterly Journal*
1008 *of the Royal Meteorological Society*, **131 (613)**, 3235–3246.

1009 Haario, H., 2010: Early rejection in metropolis-hastings. *Private communication*.

1010 Hamill, T., C. Snyder, and R. Morss, 2000: A comparison of probabilistic forecasts from bred,
1011 singular-vector, and perturbed observation ensembles. *Monthly Weather Review*, **128 (6)**,
1012 1835–1851.

1013 Harlim, J. and A. Majda, 2008: Filtering nonlinear dynamical systems with linear stochastic
1014 models. *Nonlinearity*, **21**, 1281.

1015 Harvey, A., 1991: *Forecasting, structural time series models and the Kalman filter*. Cam-
1016 bridge Univ Pr.

1017 Hesthaven, J., S. Gottlieb, and D. Gottlieb, 2007: *Spectral methods for time-dependent*
1018 *problems*, Vol. 21. Cambridge Univ Pr.

1019 Hinze, M., R. Pinnau, M. Ulbrich, and S. Ulbrich, 2008: *Optimization with PDE constraints*.
1020 Springer Verlag.

1021 Jazwinski, A., 1970: *Stochastic processes and filtering theory*. Academic Pr.

1022 Kaipio, J. and E. Somersalo, 2005: *Statistical and computational inverse problems*. Springer
1023 Science+ Business Media, Inc.

1024 Kalman, R., 1960: A new approach to linear filtering and prediction problems. *Journal of*
1025 *basic Engineering*, **82 (Series D)**, 35–45.

1026 Kalnay, E., 2003: *Atmospheric modeling, data assimilation, and predictability*. Cambridge
1027 Univ Pr.

1028 Kelley, C., 2003: *Solving nonlinear equations with Newton’s method*, Vol. 1. Society for
1029 Industrial Mathematics.

1030 Lawless, A., N. Nichols, and S. Ballard, 2003: A comparison of two methods for developing
1031 the linearization of a shallow-water model. *Quarterly Journal of the Royal Meteorological*
1032 *Society*, **129 (589)**, 1237–1254.

1033 Lei, J., P. Bickel, and C. Snyder, 2010: Comparison of ensemble kalman filters under non-

1034 gaussianity. *Monthly Weather Review*, **138** (4), 1293–1306.

1035 Leutbecher, M., 2003: Adaptive observations, the hessian metric and singular vectors. *Proc.*
1036 *ECMWF Seminar on Recent developments in data assimilation for atmosphere and ocean,*
1037 *Reading, UK*, 8–12.

1038 Liu, N. and D. S. Oliver, 2003: Evaluation of monte carlo methods for assessing uncertainty.
1039 *SPE Journal*, **8** (2), 188–195.

1040 Lorenc, A., 1986: Analysis methods for numerical weather prediction. *Quarterly Journal of*
1041 *the Royal Meteorological Society*, **112** (474), 1177–1194.

1042 Lorenz, E., 1963: Deterministic nonperiodic flow1. *Atmos J Sci*, **20**, 130–141.

1043 Lorenz, E., 1996: Predictability: A problem partly solved. *Proc. Seminar on Predictability,*
1044 *Vol. 1*, 1–18.

1045 Majda, A., J. Harlim, and B. Gershgorin, 2010: Mathematical strategies for filtering turbu-
1046 lent dynamical systems. *DYNAMICAL SYSTEMS*, **27** (2), 441–486.

1047 Meng, Z. and F. Zhang, 2010: Tests of an ensemble kalman filter for mesoscale and regional-
1048 scale data assimilation. part iv: Comparison with 3dvar in a month-long experiment.

1049 Miller, R., M. Ghil, and F. Gauthiez, 1994: Advanced data assimilation in strongly nonlinear
1050 dynamical systems. *Journal of the Atmospheric Sciences*, **51** (8), 1037–1037.

1051 Nocedal, J. and S. Wright, 1999: *Numerical optimization*. Springer verlag.

1052 Palmer, T., R. Gelaro, J. Barkmeijer, and R. Buizza, 1998: Singular vectors, metrics, and
1053 adaptive observations. *Journal of the atmospheric sciences*, **55** (4), 633–653.

1054 Quinn, J. and H. Abarbanel, 2010: State and parameter estimation using monte carlo eval-
1055 uation of path integrals. *Quarterly Journal of the Royal Meteorological Society*.

1056 Saad, Y., 1996: *Iterative methods for sparse linear systems*. PWS Pub. Co.

1057 Snyder, T., T. Bengtsson, P. Bickel, and J. Anderson, 2008: Obstacles to high-dimensional
1058 particle filtering. *Monthly Weather Review.*, **136**, 4629–4640.

1059 Stuart, A., 2010: Inverse problems: a Bayesian perspective. *Acta Numerica*, **19** (-1), 451–

1060 559.

1061 Talagrand, O. and P. Courtier, 1987: Variational assimilation of meteorological observations
1062 with the adjoint vorticity equation. i: Theory. *Quarterly Journal of the Royal Meteorolog-*
1063 *ical Society*, **113 (478)**, 1311–1328.

1064 Tarantola, A., 2005: *Inverse problem theory and methods for model parameter estimation*.
1065 Society for Industrial Mathematics.

1066 Temam, R., 2001: *Navier-Stokes equations: theory and numerical analysis*. Amer Mathe-
1067 matical Society.

1068 Tippett, M., J. Anderson, C. Bishop, T. Hamill, and J. Whitaker, 2003: Ensemble square
1069 root filters. *Monthly weather review*, **131 (7)**, 1485–1490.

1070 Toth, Z. and E. Kalnay, 1997: Ensemble forecasting at ncep and the breeding method.
1071 *Monthly Weather Review*, **125**, 3297.

1072 Trefethen, L. and D. Bau, 1997: *Numerical linear algebra*. 50, Society for Industrial Mathe-
1073 matics.

1074 Van Leeuwen, P., 2009: Particle filtering in geophysical systems. *Monthly Weather Review*,
1075 **137**, 4089–4114.

1076 van Leeuwen, P., 2010: Nonlinear data assimilation in geosciences: an extremely efficient
1077 particle filter. *Quarterly Journal of the Royal Meteorological Society*, **136 (653)**, 1991–
1078 1999.

1079 Vogel, C., 2002: *Computational methods for inverse problems*. Society for Industrial Mathe-
1080 matics.

1081 Vogel, C. and J. Wade, 1995: Analysis of costate discretizations in parameter estimation for
1082 linear evolution equations. *SIAM journal on control and optimization*, **33 (1)**, 227–254.

1083 Zhang, M. and F. Zhang, 2012: E4dvar: Coupling an ensemble kalman filter with four-
1084 dimensional variational data assimilation in a limited-area weather prediction model.
1085 *Monthly Weather Review-Boston*, **140 (2)**, 587.

1086 Zhang, M., F. Zhang, X. Huang, and X. Zhang, 2010: Inter-comparison of an ensemble

1087 kalman filter with three-and four-dimensional variational data assimilation methods in a
1088 limited-area model over the month of june 2003. *Monthly Weather Review*.
1089 Zupanski, D., 1997: A general weak constraint applicable to operational 4dvar data assimi-
1090 lation systems. *Monthly Weather Review*, **125**, 2274–2292.

1091 **List of Tables**

1092 1 Stationary state regime, $\nu = 0.1$, $T = 2$, with $h = 0.2$ (top table), $h = 1$ (mid-
1093 dle), and $h = 2$ (bottom). The first, third, fourth and fifth columns are the
1094 norm difference, $e = \|M - m\|/\|M\|$, where M is the mean of the posterior
1095 distribution (MCMC), the truth, the observation, or the MAP estimator and
1096 m is the mean obtained from the various methods. The second column is the
1097 norm difference, $e = \|\text{var}[u] - \text{var}[U]\|/\|\text{var}[u]\|$ where var indicates the vari-
1098 ance, u is sampled from the posterior (via MCMC), and U is the approximate
1099 state obtained from the various methods. 50

1100 2 Same as Table 1, except for strongly chaotic regime with $\nu = 0.01$, $T = 0.2$,
1101 and $h = 0.02$ (top), 0.1 (middle) and 0.2 (bottom). 51

1102 3 Same as Table 2, except $T = 1$, and $h = 0.2$ (top) and $h = 0.5$ (bottom).
1103 The variance is omitted from the 4DVAR solutions here, because we are
1104 unable to attain solution with zero derivative. We must note here that we
1105 have taken the approach of differentiating and then discretizing. Therefore,
1106 over longer time intervals such as this, the error between the discretization of
1107 the analytical derivative and derivative of the finite-dimensional discretized
1108 forward map accumulates and the derivative of the objective function is no
1109 longer well-defined because of this error. Nonetheless, we confirm that we do
1110 obtain the MAP estimator because the MCMC run does not yield any point
1111 of higher probability. 52

1112 4 The data of unstable algorithms from Table 2 ($\nu = 0.01$, $T = 0.2$) are re-
1113 produced above (with $h = 0.02$ (top) and $h = 0.2$ (bottom)), along with the
1114 respective stabilized versions in brackets. Here the stabilized versions usually
1115 perform worse. Note that over longer time scales, the unstabilized version will
1116 diverge from the truth, while the stabilized one remains close. 53

| | | | |
|------|---|---|----|
| 1117 | 5 | Same as Table 4, except $T = 5h = 1$ and $h = 0.2$. [3DVAR] performs better | |
| 1118 | | with respect to the mean. | 54 |
| 1119 | 6 | Same as Table 5, except $h = 0.5$. All stabilized algorithms now perform better | |
| 1120 | | with respect to the mean. [LRExKF] above uses 50 eigenvectors in the low | |
| 1121 | | rank representation, and performs <i>worse</i> for larger number, indicating that | |
| 1122 | | the improvement is due largely to the FDF component. The stable FDF | |
| 1123 | | data are included here as well, since FDF is now competitive as the optimal | |
| 1124 | | algorithm in terms of mean estimator. This is expected to persist for larger | |
| 1125 | | time windows and lower frequency observations, since the LRExKF is outside | |
| 1126 | | of the regime of validity, as shown in Figure 4. | 55 |

| $h = 0.2$ | e_{mean} | $e_{variance}$ | e_{truth} | e_{obs} | e_{map} |
|-------------------|-------------|----------------|-------------|-----------|-------------|
| MCMC($t = 0$) | 0 | 0 | 0.17177 | 0.819094 | 0.00153443 |
| 4DVAR($t = 0$) | 0.00153523 | 0.00620345 | 0.185876 | 0.740612 | 0 |
| MCMC($t = T$) | 0 | 0 | 0.0164605 | 0.558026 | 5.17207e-05 |
| 4DVAR($t = T$) | 5.1723e-05 | 0.00459055 | 0.0164618 | 0.558024 | 0 |
| 3DVAR | 0.138652 | 108.516 | 0.13738 | 0.54585 | 0.138646 |
| FDF | 0.00173093 | 0.423299 | 0.0153513 | 0.558228 | 0.00172455 |
| LRExKF | 6.34566e-05 | 0.00320937 | 0.0164796 | 0.558022 | 2.22202e-05 |
| EnKF | 0.00359669 | 0.119076 | 0.0158585 | 0.558032 | 0.00362309 |
| truth ($t = 0$) | 0.17177 | - | 0 | 0.816333 | 0.156072 |
| truth ($t = T$) | 0.0164605 | - | 0 | 0.713754 | 0.0164342 |
| $h = 1$ | e_{mean} | $e_{variance}$ | e_{truth} | e_{obs} | e_{map} |
| MCMC($t = 0$) | 0 | 0 | 0.295424 | 0.791832 | 0.00110927 |
| 4DVAR($t = 0$) | 0.00110969 | 0.00375462 | 0.333225 | 0.748439 | 0 |
| MCMC($t = T$) | 0 | 0 | 0.028831 | 0.662342 | 0.00016539 |
| 4DVAR($t = T$) | 0.000165408 | 0.00896381 | 0.0287779 | 0.662373 | 0 |
| 3DVAR | 0.128956 | 41.6646 | 0.139419 | 0.646462 | 0.128929 |
| FDF | 0.00400194 | 0.458239 | 0.031512 | 0.654203 | 0.00403853 |
| LRExKF | 0.000165666 | 0.00267976 | 0.0287787 | 0.65413 | 1.84537e-05 |
| EnKF | 0.00289635 | 0.122461 | 0.0301991 | 0.654205 | 0.00285458 |
| truth ($t = 0$) | 0.295424 | - | 0 | 0.780891 | 0.27957 |
| truth ($t = T$) | 0.028831 | - | 0 | 0.77011 | 0.0287068 |
| $h = 2$ | e_{mean} | $e_{variance}$ | e_{truth} | e_{obs} | e_{map} |
| MCMC($t = 0$) | 0 | 0 | 0.32043 | 0.747756 | 0.000965003 |
| 4DVAR($t = 0$) | 0.000965294 | 0.00384239 | 0.357404 | 0.633977 | 0 |
| MCMC($t = T$) | 0 | 0 | 0.03871 | 0.68846 | 0.000208273 |
| 4DVAR($t = T$) | 0.000208299 | 0.00250571 | 0.0386606 | 0.68846 | 0 |
| 3DVAR | 0.105535 | 35.9905 | 0.108918 | 0.684345 | 0.10548 |
| FDF | 0.00177839 | 0.475338 | 0.0387006 | 0.688477 | 0.00173164 |
| LRExKF | 0.0002106 | 0.00272041 | 0.0386602 | 0.68846 | 2.991e-06 |
| EnKF | 0.00319756 | 0.106976 | 0.0385305 | 0.688464 | 0.00312047 |
| truth ($t = 0$) | 0.32043 | - | 0 | 0.771936 | 0.299957 |
| truth ($t = T$) | 0.03871 | - | 0 | 0.688664 | 0.038578 |

TABLE 1. Stationary state regime, $\nu = 0.1$, $T = 2$, with $h = 0.2$ (top table), $h = 1$ (middle), and $h = 2$ (bottom). The first, third, fourth and fifth columns are the norm difference, $e = \|M - m\|/\|M\|$, where M is the mean of the posterior distribution (MCMC), the truth, the observation, or the MAP estimator and m is the mean obtained from the various methods. The second column is the norm difference, $e = \|\text{var}[u] - \text{var}[U]\|/\|\text{var}[u]\|$ where var indicates the variance, u is sampled from the posterior (via MCMC), and U is the approximate state obtained from the various methods.

| $h = 0.02$ | e_{mean} | $e_{variance}$ | e_{truth} | e_{obs} | e_{map} |
|-------------------|-------------|----------------|-------------|-----------|-------------|
| MCMC($t = 0$) | 0 | 0 | 0.0331468 | 0.337233 | 0.000731645 |
| 4DVAR($t = 0$) | 0.000731491 | 0.0932748 | 0.0331531 | 0.310411 | 0 |
| MCMC($t = T$) | 0 | 0 | 0.0423943 | 0.32224 | 0.00130105 |
| 4DVAR($t = T$) | 0.00130112 | 0.045048 | 0.042431 | 0.322306 | 0 |
| 3DVAR | 0.0634553 | 6.34057 | 0.063289 | 0.321959 | 0.0634026 |
| FDF | 0.165732 | 28.9155 | 0.175397 | 0.307159 | 0.165844 |
| LRExKF | 0.00599214 | 0.030054 | 0.0416529 | 0.322277 | 0.0054415 |
| EnKF | 0.035271 | 0.274428 | 0.0523566 | 0.323074 | 0.0354624 |
| truth ($t = 0$) | 0.0331468 | - | 0 | 0.335933 | 0.0361395 |
| truth ($t = T$) | 0.0423943 | - | 0 | 0.339539 | 0.0429021 |
| $h = 0.1$ | e_{mean} | $e_{variance}$ | e_{truth} | e_{obs} | e_{map} |
| MCMC($t = 0$) | 0 | 0 | 0.0496982 | 0.294743 | 0.000815864 |
| 4DVAR($t = 0$) | 0.000815762 | 0.0287498 | 0.0497009 | 0.280425 | 0 |
| MCMC($t = T$) | 0 | 0 | 0.0698665 | 0.35798 | 0.00306996 |
| 4DVAR($t = T$) | 0.00307105 | 0.0118785 | 0.06983 | 0.358094 | 0 |
| 3DVAR | 0.159393 | 2.2339 | 0.203165 | 0.374188 | 0.159658 |
| FDF | 0.200044 | 13.259 | 0.215136 | 0.308921 | 0.200045 |
| LRExKF | 0.023073 | 0.0313686 | 0.0766505 | 0.357915 | 0.0215118 |
| EnKF | 0.0539001 | 0.174878 | 0.109402 | 0.358301 | 0.0543726 |
| truth ($t = 0$) | 0.0496982 | - | 0 | 0.303742 | 0.0541391 |
| truth ($t = T$) | 0.0698665 | - | 0 | 0.368335 | 0.0705546 |
| $h = 0.2$ | e_{mean} | $e_{variance}$ | e_{truth} | e_{obs} | e_{map} |
| MCMC($t = 0$) | 0 | 0 | 0.0459125 | 0.293686 | 0.00122936 |
| 4DVAR($t = 0$) | 0.00183617 | 0.0231955 | 0.0462013 | 0.281137 | 0 |
| MCMC($t = T$) | 0 | 0 | 0.072738 | 0.352456 | 0.00385795 |
| 4DVAR($t = T$) | 0.00386162 | 0.0196227 | 0.0723178 | 0.352145 | 0 |
| 3DVAR | 0.285461 | 1.72154 | 0.300853 | 0.38443 | 0.286161 |
| FDF | 0.202274 | 10.7793 | 0.203287 | 0.316707 | 0.202862 |
| LRExKF | 0.0750908 | 0.0547417 | 0.0886932 | 0.35073 | 0.0726792 |
| EnKF | 0.0964053 | 0.0948967 | 0.113806 | 0.352625 | 0.0962341 |
| truth ($t = 0$) | 0.0459125 | - | 0 | 0.301899 | 0.0496251 |
| truth ($t = T$) | 0.072738 | - | 0 | 0.368331 | 0.0720492 |

TABLE 2. Same as Table 1, except for strongly chaotic regime with $\nu = 0.01$, $T = 0.2$, and $h = 0.02$ (top), 0.1 (middle) and 0.2 (bottom).

| $h = 0.2$ | e_{mean} | $e_{variance}$ | e_{truth} | e_{obs} | e_{map} |
|-------------------|------------|----------------|-------------|-----------|------------|
| MCMC($t = 0$) | 0 | 0 | 0.0322397 | 0.294722 | 0.00122667 |
| 4DVAR($t = 0$) | 0.00122657 | - | 0.0316494 | 0.280742 | 0 |
| MCMC($t = T$) | 0 | 0 | 0.0480924 | 0.27997 | 0.00484999 |
| 4DVAR($t = T$) | 0.0048519 | - | 0.0474821 | 0.279995 | 0 |
| 3DVAR | 0.35571 | 3.17803 | 0.357351 | 0.419614 | 0.35557 |
| FDF | 0.141426 | 19.2983 | 0.152064 | 0.260197 | 0.142169 |
| LRExKF | 0.101179 | 0.28308 | 0.0900697 | 0.291704 | 0.101287 |
| EnKF | 0.202724 | 0.230518 | 0.173947 | 0.320302 | 0.202665 |
| truth ($t = 0$) | 0.0322397 | - | 0 | 0.303376 | 0.0272922 |
| truth ($t = T$) | 0.0480924 | - | 0 | 0.281553 | 0.0474964 |
| $h = 0.5$ | e_{mean} | $e_{variance}$ | e_{truth} | e_{obs} | e_{map} |
| MCMC($t = 0$) | 0 | 0 | 0.0318531 | 0.293871 | 0.0030989 |
| 4DVAR($t = 0$) | 0.00309769 | - | 0.0313382 | 0.280152 | 0 |
| MCMC($t = T$) | 0 | 0 | 0.0460821 | 0.288812 | 0.00831516 |
| 4DVAR($t = T$) | 0.00831886 | - | 0.0448424 | 0.289043 | 0 |
| 3DVAR | 0.458527 | 1.8214 | 0.45353 | 0.487658 | 0.460144 |
| FDF | 0.189832 | 11.4573 | 0.19999 | 0.25111 | 0.191364 |
| LRExKF | 0.644427 | 0.325391 | 0.650004 | 1.22145 | 0.646233 |
| EnKF | 0.901703 | 0.554611 | 0.895878 | 0.908817 | 0.902438 |
| truth ($t = 0$) | 0.0318531 | - | 0 | 0.303185 | 0.0269929 |
| truth ($t = T$) | 0.0460821 | - | 0 | 0.294524 | 0.0448046 |

TABLE 3. Same as Table 2, except $T = 1$, and $h = 0.2$ (top) and $h = 0.5$ (bottom). The variance is omitted from the 4DVAR solutions here, because we are unable to attain solution with zero derivative. We must note here that we have taken the approach of differentiating and then discretizing. Therefore, over longer time intervals such as this, the error between the discretization of the analytical derivative and derivative of the finite-dimensional discretized forward map accumulates and the derivative of the objective function is no longer well-defined because of this error. Nonetheless, we confirm that we do obtain the MAP estimator because the MCMC run does not yield any point of higher probability.

| h=0.02 | e_{mean} | $e_{variance}$ | e_{truth} | e_{obs} | e_{map} |
|----------|------------|----------------|-------------|-----------|-----------|
| 3DVAR | 0.0634553 | 6.34057 | 0.063289 | 0.321959 | 0.0634026 |
| [3DVAR] | 0.142759 | 22.2668 | 0.153141 | 0.309838 | 0.143005 |
| EnKF | 0.035271 | 0.274428 | 0.0523566 | 0.323074 | 0.0354624 |
| [EnKF] | 0.167776 | 28.1196 | 0.175359 | 0.304352 | 0.167919 |
| h=0.2 | e_{mean} | $e_{variance}$ | e_{truth} | e_{obs} | e_{map} |
| 3DVAR | 0.285461 | 1.72154 | 0.300853 | 0.38443 | 0.286161 |
| [3DVAR] | 0.195222 | 6.33608 | 0.204883 | 0.339108 | 0.196339 |
| LRExKF | 0.0750908 | 0.0547417 | 0.0886932 | 0.35073 | 0.0726792 |
| [LRExKF] | 0.156973 | 7.64123 | 0.169354 | 0.310298 | 0.156596 |
| EnKF | 0.137844 | 0.372259 | 0.159744 | 0.353934 | 0.137969 |
| [EnKF] | 0.248081 | 6.34903 | 0.267746 | 0.368067 | 0.249475 |

TABLE 4. The data of unstable algorithms from Table 2 ($\nu = 0.01$, $T = 0.2$) are reproduced above (with $h = 0.02$ (top) and $h = 0.2$ (bottom)), along with the respective stabilized versions in brackets. Here the stabilized versions usually perform worse. Note that over longer time scales, the unstabilized version will diverge from the truth, while the stabilized one remains close.

| h=0.2 | e_{mean} | $e_{variance}$ | e_{truth} | e_{obs} | e_{map} |
|----------|------------|----------------|-------------|-----------|-----------|
| 3DVAR | 0.35571 | 3.17803 | 0.357351 | 0.419614 | 0.35557 |
| [3DVAR] | 0.131964 | 11.5997 | 0.135572 | 0.277895 | 0.133265 |
| LRExKF | 0.101179 | 0.28308 | 0.0900697 | 0.291704 | 0.101287 |
| [LRExKF] | 0.12962 | 16.3692 | 0.13592 | 0.256617 | 0.129742 |
| EnKF | 0.0736613 | 0.276947 | 0.0755232 | 0.282247 | 0.0742144 |
| [EnKF] | 0.1231 | 14.8557 | 0.133171 | 0.261061 | 0.124203 |

TABLE 5. Same as Table 4, except $T = 5h = 1$ and $h = 0.2$. [3DVAR] performs better with respect to the mean.

| h=0.5 | e_{mean} | $e_{variance}$ | e_{truth} | e_{obs} | e_{map} |
|----------|------------|----------------|-------------|-----------|-----------|
| 3DVAR | 0.458527 | 1.8214 | 0.45353 | 0.487658 | 0.460144 |
| [3DVAR] | 0.27185 | 6.62328 | 0.285351 | 0.307263 | 0.274663 |
| LRExKF | 0.644427 | 0.325391 | 0.650004 | 1.22145 | 0.646233 |
| [LRExKF] | 0.201327 | 11.2449 | 0.207526 | 0.244101 | 0.201081 |
| EnKF | 0.901703 | 0.554611 | 0.895878 | 0.908817 | 0.902438 |
| [EnKF] | 0.169262 | 4.07238 | 0.17874 | 0.244571 | 0.170245 |
| FDF | 0.189832 | 11.4573 | 0.19999 | 0.25111 | 0.191364 |

TABLE 6. Same as Table 5, except $h = 0.5$. All stabilized algorithms now perform better with respect to the mean. [LRExKF] above uses 50 eigenvectors in the low rank representation, and performs *worse* for larger number, indicating that the improvement is due largely to the FDF component. The stable FDF data are included here as well, since FDF is now competitive as the optimal algorithm in terms of mean estimator. This is expected to persist for larger time windows and lower frequency observations, since the LRExKF is outside of the regime of validity, as shown in Figure 4.

1127 **List of Figures**

1128 1 Low Reynolds number, stationary solution regime ($\nu = 0.1$). The vorticity,
 1129 $w(0)$ (left) of the smoothing distribution at $t = 0$, and its Fourier coefficients
 1130 (right), are presented for $T = 10h = 2$. The top and bottom rows are the
 1131 MCMC sample mean and the truth. The MAP estimator is not distinguish-
 1132 able from the mean by eye and so is not displayed. The prior mean is taken
 1133 as a draw from the prior, and hence is not as smooth as the initial condition.
 1134 It is the influence of the prior which makes the MAP estimator and mean
 1135 rough, although structurally the same as the truth (the solution operator is
 1136 smoothing, so these fluctuations are immediately smoothed out - see Fig. 2). 59

1137 2 Low Reynolds number, stationary solution regime ($\nu = 0.1$). The vorticity,
 1138 $w(T)$ (left) of the filtering distribution at $t = T$, and its Fourier coefficients
 1139 (right), are presented for $T = 10h = 2$. Only the MCMC sample mean is
 1140 shown, since the solutions have been smoothed out and the difference between
 1141 the MAP, mean, and truth is imperceptible. 60

1142 3 The MCMC histogram at $t = 0$ (left) and $t = T = 10h = 2$ (right) together
 1143 with the Gaussian approximation obtained from 4DVAR for low Reynolds
 1144 number, stationary state regime ($\nu = 0.1$). 61

| | | | |
|------|---|--|----|
| 1145 | 4 | The left panel is the average velocity spectrum on the attractor for $\nu = 0.01$. The right panel shows the difference between (a) and (b) where: (a) is the difference of the truth $u^\dagger(t)$ with a solution $u_\tau(t)$ initially perturbed in the di- rection of the dominant local Lyapunov vectors v_τ , on time-interval of length τ , with $\tau = 0.02, 0.2$, and 0.5 (thus $u_\tau(0) = u^\dagger(0) + \varepsilon v_\tau$); and (b) is the evolu- tion of that perturbation under the linearized model $U_\tau(t) = D\Psi(u^\dagger(0); t)\varepsilon v_\tau$. The magnitude of perturbation ε is determined by the projection of the initial posterior covariance in the direction v_τ . The difference plotted thus indicates differences between linear and nonlinear evolution with the the direction of the initial perturbations chosen to maximize growth and with size of the initial perturbations commensurate with the prevalent uncertainty. The relative er- ror $ (u_\tau(\tau) - u^\dagger(\tau)) - U_\tau(\tau) / U_\tau(\tau) $ (in l^2) is $0.01, 0.15$, and 0.42 , respectively, for the three chosen values of increasing τ | 62 |
| 1158 | 5 | The MCMC mean, as in Fig. 1 for high Reynolds number, strongly chaotic solution regime. $\nu = 0.01, T = 10h = 0.2, t = 0$ (top) and $t = T$ (bottom). . . | 63 |
| 1160 | 6 | Same as Fig. 3, except for strongly chaotic regime, $\nu = 0.01, T = 0.2$, and $h = 0.02$. The top is mode $u_{1,1}$ and the bottom shows mode $u_{5,5}$ | 64 |
| 1162 | 7 | The left and right panels, respectively, show the posterior and prior of the covariance from converged innovation statistics from the cycled 3DVAR algo- rithm, in comparison to the converged covariance from the FDF algorithm, and the posterior distribution. | 65 |
| 1166 | 8 | Example of an unstable trajectory for 3DVAR with $\nu = 0.01, h = 0.2$. The top left plot shows the norm-squared error between the estimated mean, $m(t_n) =$ \hat{m}_n , and the truth, $u^\dagger(t_n)$, in comparison to the preferred upper bound (i.e. the total observation error $\text{tr}(\Gamma)$, (21)) and the lower bound $\text{tr}[K_n\Gamma K_n^*]$ (20). The other three plots show the estimator, $m(t)$, together with the truth, $u^\dagger(t)$, and the observations, y_n for a few individual modes. | 66 |

| | | | |
|------|----|--|----|
| 1172 | 9 | Example of a variance-inflated stabilized trajectory ($\mathcal{C}_0 \rightarrow \frac{1}{\epsilon}\mathcal{C}_0$) for [3DVAR] | |
| 1173 | | with the same external parameters as in Fig. 8. Panels are the same as in | |
| 1174 | | Fig. 8. | 67 |
| 1175 | 10 | Example of an unstable trajectory for LRExKF with $\nu = 0.01, h = 0.5$. Panels | |
| 1176 | | are the same as in Fig. 8. | 68 |
| 1177 | 11 | Example of a variance-inflated stabilized trajectory (updated with model | |
| 1178 | | b from Section 2 on the complement of the low-rank approximation) for | |
| 1179 | | [LRExKF] with the same external parameters as in Fig. 10. Panels are | |
| 1180 | | the same as in Fig. 10. | 69 |

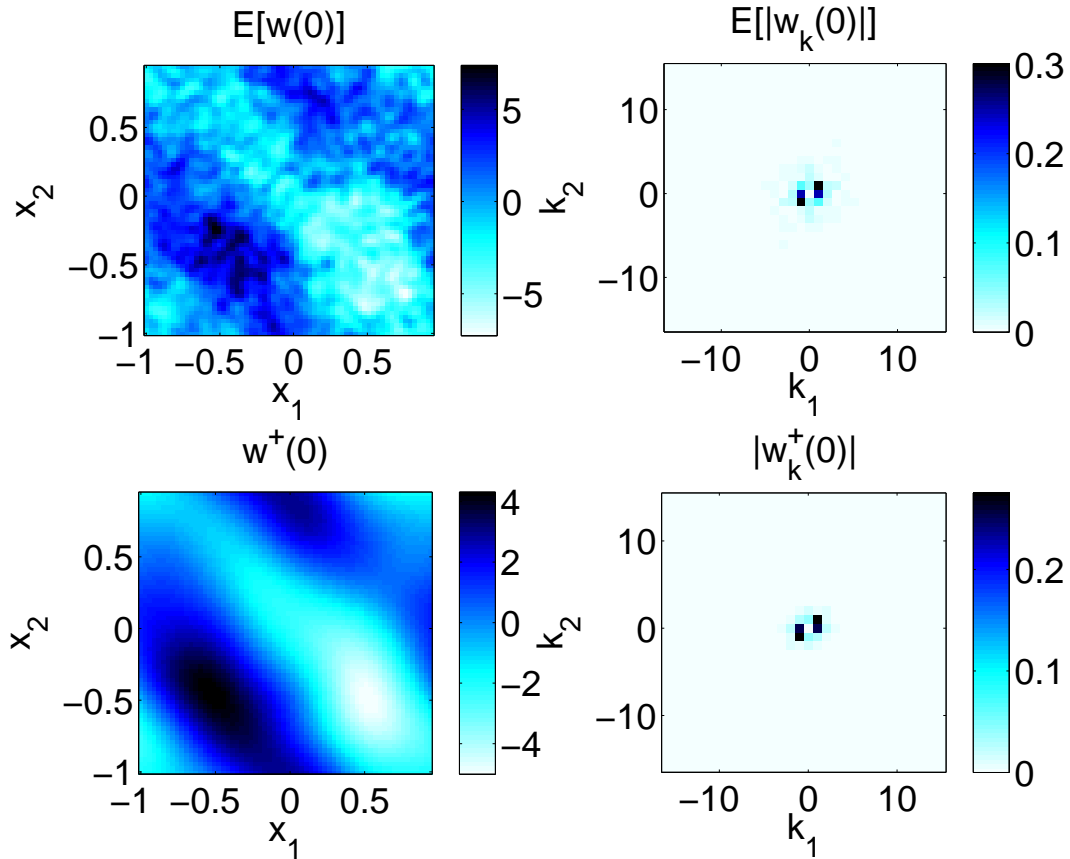


FIG. 1. Low Reynolds number, stationary solution regime ($\nu = 0.1$). The vorticity, $w(0)$ (left) of the smoothing distribution at $t = 0$, and its Fourier coefficients (right), are presented for $T = 10h = 2$. The top and bottom rows are the MCMC sample mean and the truth. The MAP estimator is not distinguishable from the mean by eye and so is not displayed. The prior mean is taken as a draw from the prior, and hence is not as smooth as the initial condition. It is the influence of the prior which makes the MAP estimator and mean rough, although structurally the same as the truth (the solution operator is smoothing, so these fluctuations are immediately smoothed out - see Fig. 2).

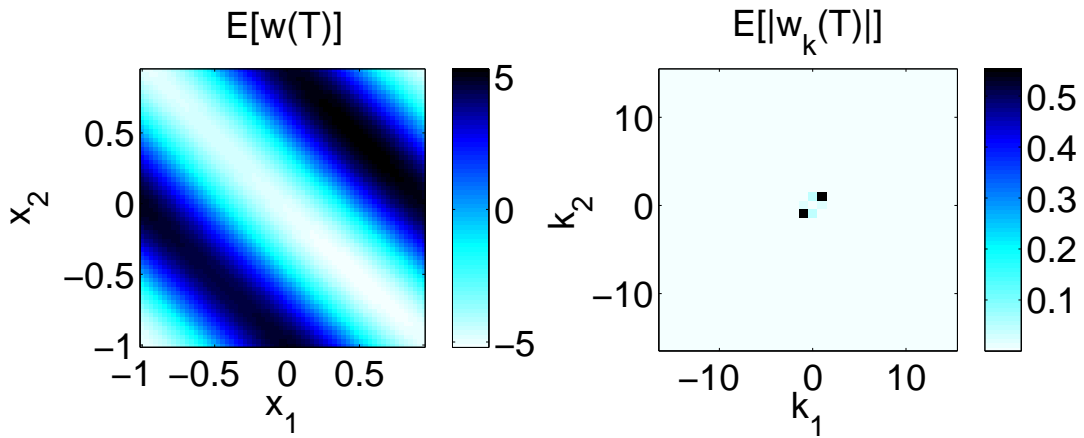


FIG. 2. Low Reynolds number, stationary solution regime ($\nu = 0.1$). The vorticity, $w(T)$ (left) of the filtering distribution at $t = T$, and its Fourier coefficients (right), are presented for $T = 10h = 2$. Only the MCMC sample mean is shown, since the solutions have been smoothed out and the difference between the MAP, mean, and truth is imperceptible.

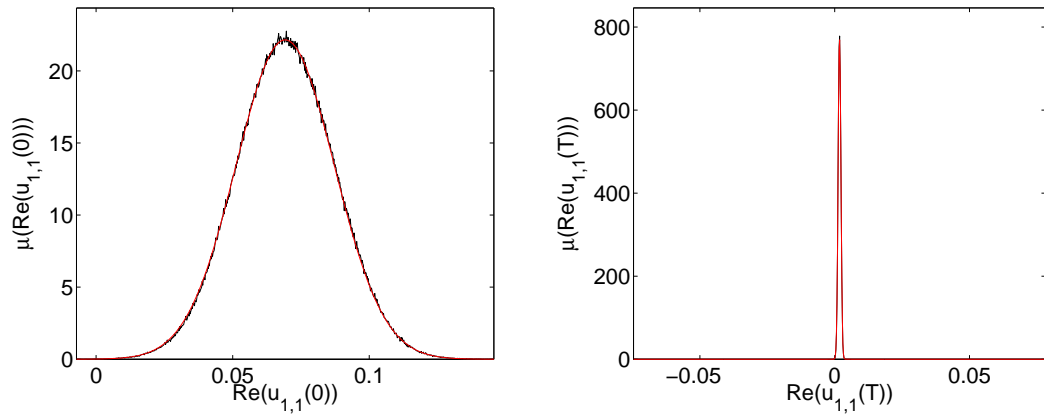


FIG. 3. The MCMC histogram at $t = 0$ (left) and $t = T = 10h = 2$ (right) together with the Gaussian approximation obtained from 4DVAR for low Reynolds number, stationary state regime ($\nu = 0.1$).

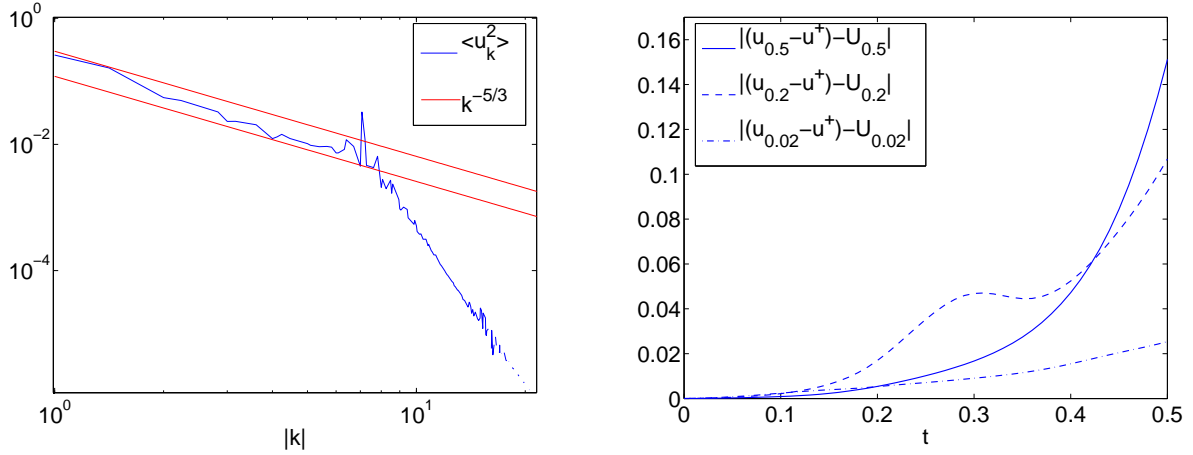


FIG. 4. The left panel is the average velocity spectrum on the attractor for $\nu = 0.01$. The right panel shows the difference between (a) and (b) where: (a) is the difference of the truth $u^\dagger(t)$ with a solution $u_\tau(t)$ initially perturbed in the direction of the dominant local Lyapunov vectors v_τ , on time-interval of length τ , with $\tau = 0.02, 0.2$, and 0.5 (thus $u_\tau(0) = u^\dagger(0) + \varepsilon v_\tau$); and (b) is the evolution of that perturbation under the linearized model $U_\tau(t) = D\Psi(u^\dagger(0); t)\varepsilon v_\tau$. The magnitude of perturbation ε is determined by the projection of the initial posterior covariance in the direction v_τ . The difference plotted thus indicates differences between linear and nonlinear evolution with the the direction of the initial perturbations chosen to maximize growth and with size of the initial perturbations commensurate with the prevalent uncertainty. The relative error $|(u_\tau(\tau) - u^\dagger(\tau)) - U_\tau(\tau)|/|U_\tau(\tau)|$ (in l^2) is 0.01, 0.15, and 0.42, respectively, for the three chosen values of increasing τ .

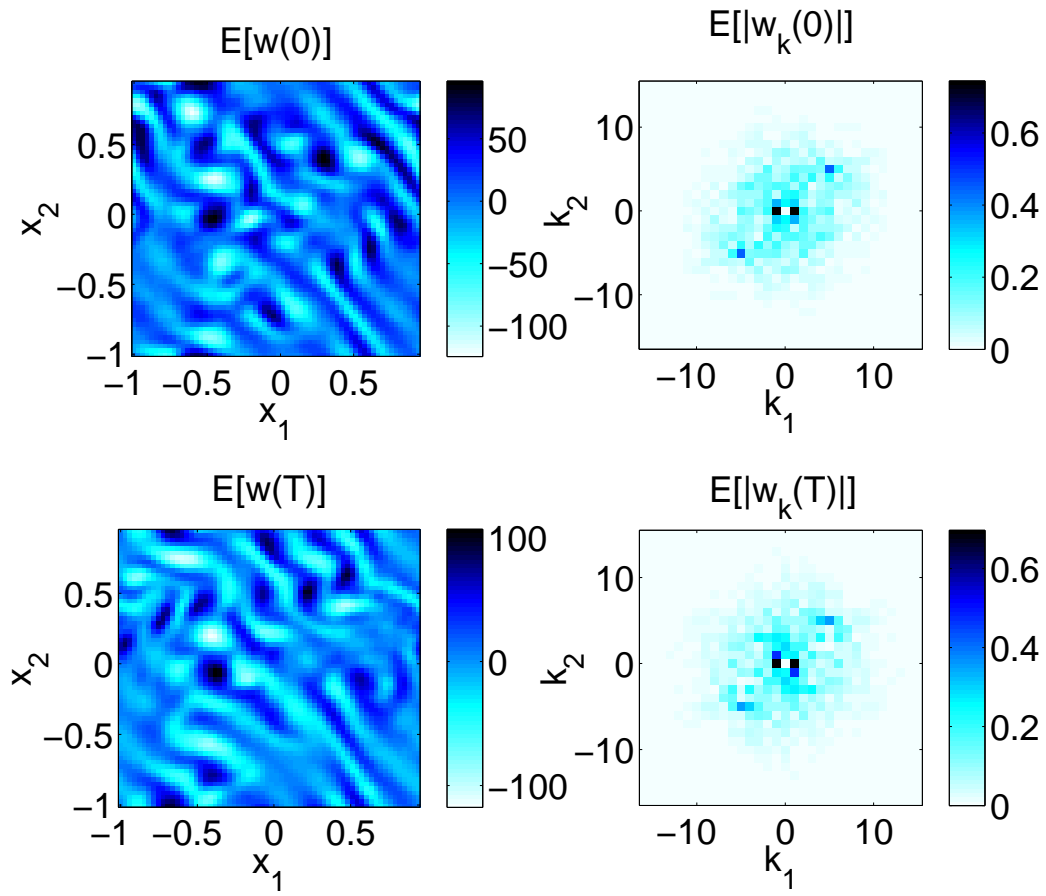


FIG. 5. The MCMC mean, as in Fig. 1 for high Reynolds number, strongly chaotic solution regime. $\nu = 0.01, T = 10h = 0.2, t = 0$ (top) and $t = T$ (bottom).

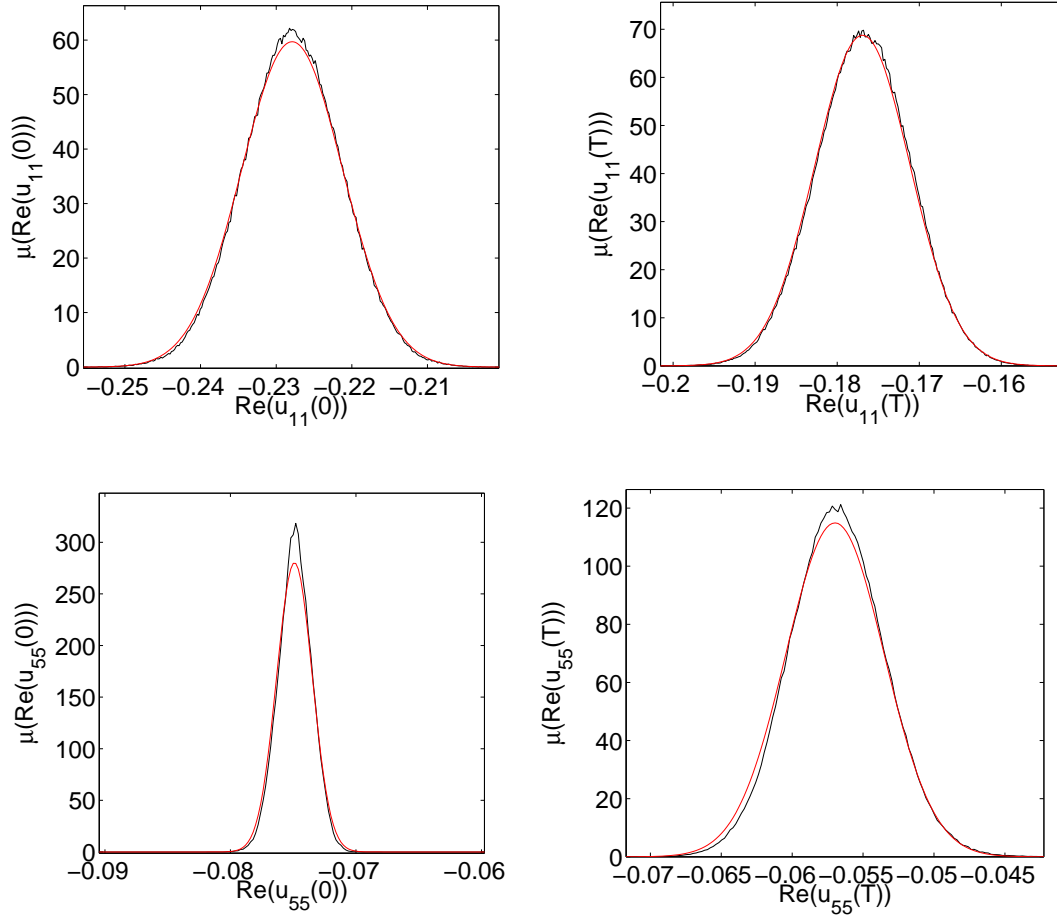


FIG. 6. Same as Fig. 3, except for strongly chaotic regime, $\nu = 0.01$, $T = 0.2$, and $h = 0.02$. The top is mode $u_{1,1}$ and the bottom shows mode $u_{5,5}$.

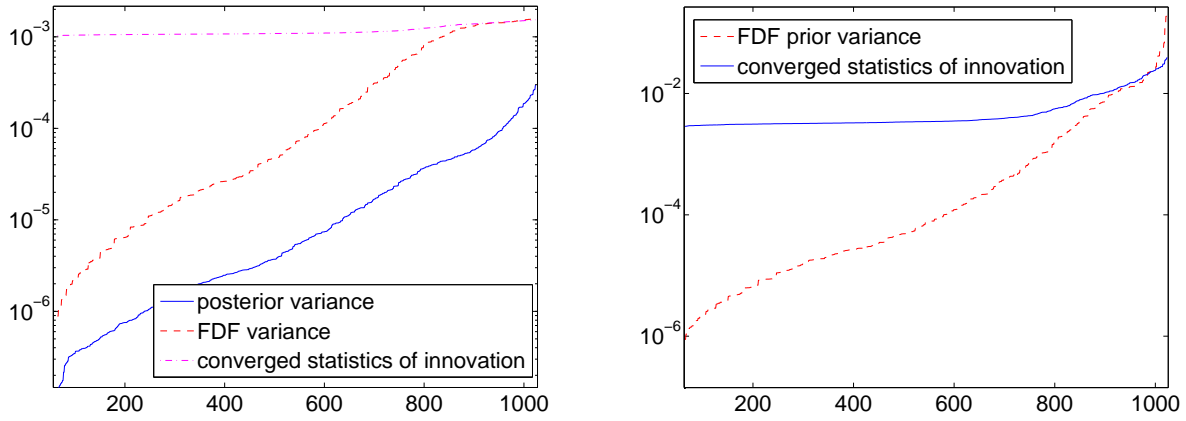


FIG. 7. The left and right panels, respectively, show the posterior and prior of the covariance from converged innovation statistics from the cycled 3DVAR algorithm, in comparison to the converged covariance from the FDF algorithm, and the posterior distribution.

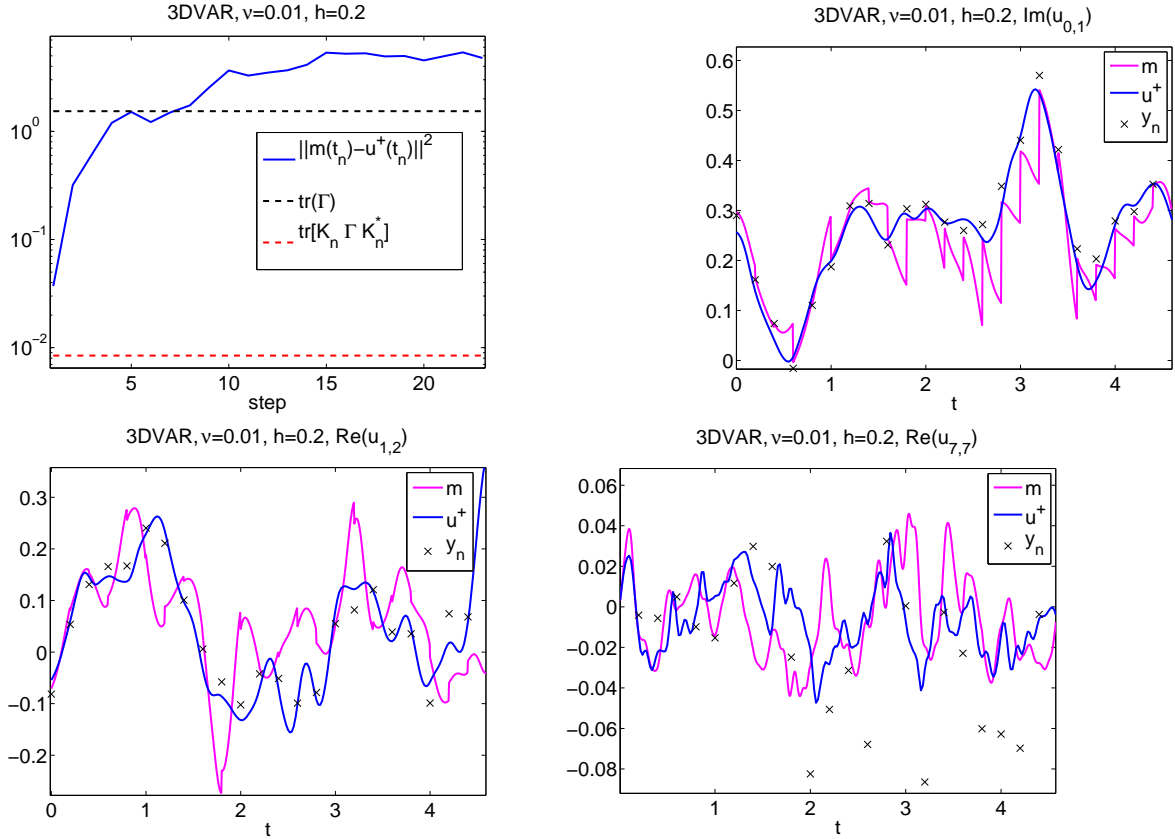


FIG. 8. Example of an unstable trajectory for 3DVAR with $\nu = 0.01, h = 0.2$. The top left plot shows the norm-squared error between the estimated mean, $m(t_n) = \hat{m}_n$, and the truth, $u^\dagger(t_n)$, in comparison to the preferred upper bound (i.e. the total observation error $\text{tr}(\Gamma)$, (21)) and the lower bound $\text{tr}[K_n \Gamma K_n^*]$ (20). The other three plots show the estimator, $m(t)$, together with the truth, $u^\dagger(t)$, and the observations, y_n for a few individual modes.

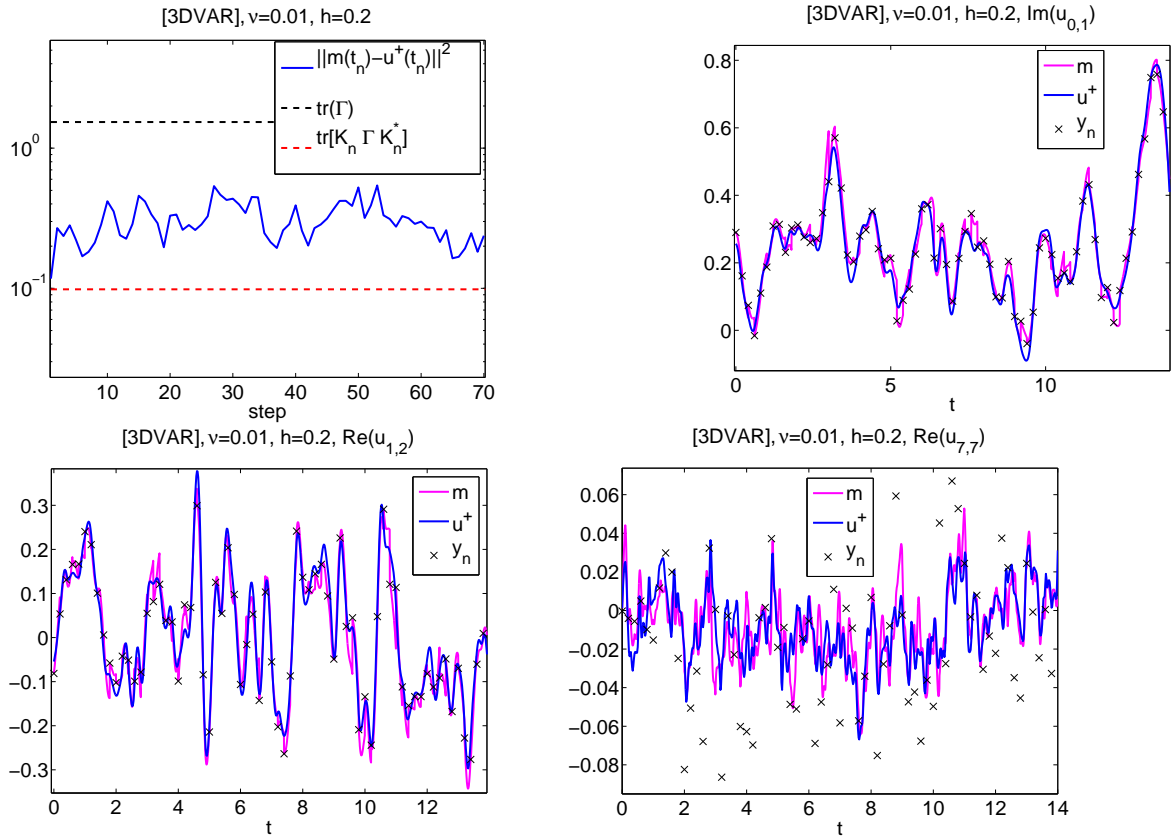


FIG. 9. Example of a variance-inflated stabilized trajectory ($\mathcal{C}_0 \rightarrow \frac{1}{\epsilon} \mathcal{C}_0$) for [3DVAR] with the same external parameters as in Fig. 8. Panels are the same as in Fig. 8.

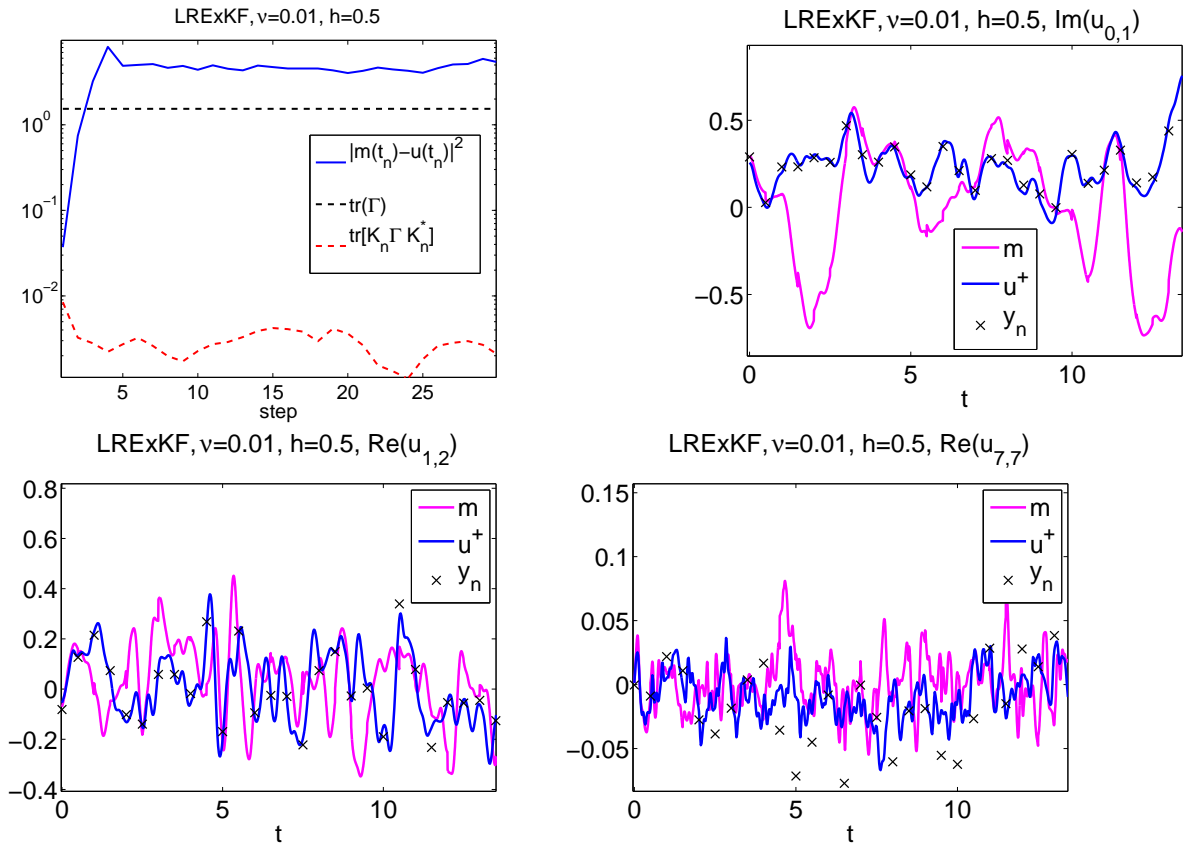


FIG. 10. Example of an unstable trajectory for LRExKF with $\nu = 0.01$, $h = 0.5$. Panels are the same as in Fig. 8.

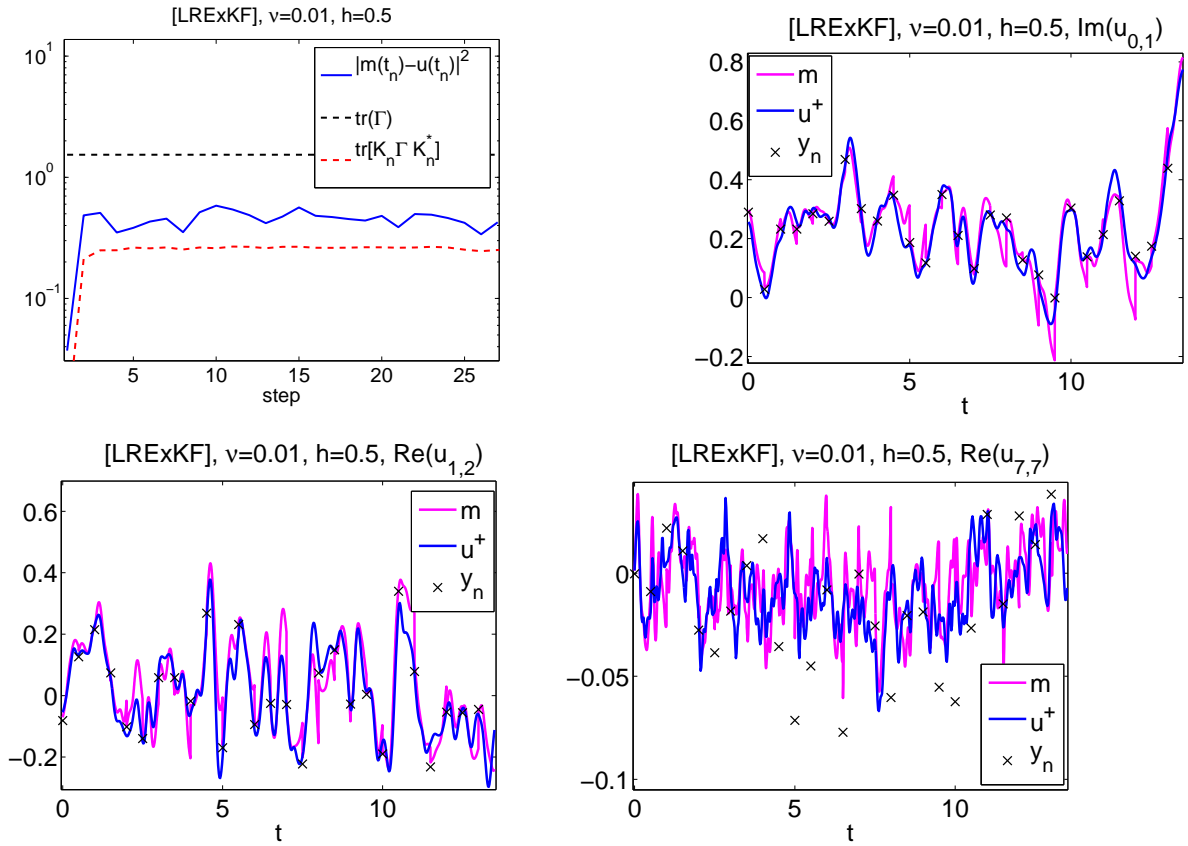


FIG. 11. Example of a variance-inflated stabilized trajectory (updated with model b from Section 2 on the complement of the low-rank approximation) for [LRExKF] with the same external parameters as in Fig. 10. Panels are the same as in Fig. 10.

